Contrib Mineral Petrol
DOI 10.1007/s00410-013-0916-z

ORIGINAL PAPER

Enrichment of Rare Earth Elements during magmatic and post-magmatic processes: a case study from the Loch Loyal Syenite Complex, northern Scotland

A. S. Walters · K. M. Goodenough · H. S. R. Hughes · N. M. W. Roberts · A. G. Gunn · J. Rushton · A. Lacinska

Received: 27 November 2012 / Accepted: 19 June 2013

Abstract Concern about security of supply of critical elements used in new technologies, such as the Rare Earth Elements (REE), means that it is increasingly important to understand the processes by which they are enriched in crustal settings. High REE contents are found in syenite-dominated alkaline complexes intruded along the Moine Thrust Zone, a major collisional zone in north-west Scotland. The most northerly of these is the Loch Loyal Syenite Complex, which comprises three separate intrusions. One of these, the Cnoc nan Cuilean intrusion, contains two mappable zones: a Mixed Syenite Zone in which mafic melasyenite is mixed and mingled with leucosyenite and a Massive Leucosyenite Zone. Within the Mixed Syenite Zone, hydrothermal activity is evident in the form of narrow altered veins dominated by biotite and magnetite; these are poorly exposed and their lateral extent is uncertain. The REE mineral allanite is relatively abundant in the melasyenite and is extremely enriched in the biotite–magnetite veins, which have up to 2 % total rare earth oxides in bulk rock analyses. An overall model for development of this intrusion can be divided into three episodes: (1) generation of a Light Rare Earth Element (LREE)-enriched parental magma due to enrichment of the mantle source by subduction of pelagic carbonates; (2) early crystallisation of allanite in melasyenite, due to the saturation of the magma in the LREE; and (3) hydrothermal alteration, in three different episodes identified by petrography and mineral chemistry, generating the intense enrichment of REE in the biotite–magnetite veins. Dating of allanite and titanite in the biotite–magnetite veins gives ages of c. 426 Ma, overlapping with previously published crystallisation ages for zircon in the syenite.

Keywords Rare Earth Elements · Post-collisional · Syenite · Allanite · Hydrothermal alteration

Communicated by F. Poitrasson.

Electronic supplementary material The online version of this article (doi:10.1007/s00410-013-0916-z) contains supplementary material, which is available to authorized users.

A. S. Walters · A. G. Gunn · J. Rushton · A. Lacinska
British Geological Survey, Nicker Hill, Keyworth, Nottingham NG12 5GG, UK

K. M. Goodenough (✉)
British Geological Survey, West Mains Road, Edinburgh EH9 3LA, UK
e-mail: kmgo@bgs.ac.uk

H. S. R. Hughes
School of Earth and Ocean Sciences, Cardiff University, Park Place, Cardiff CF10 3AT, UK

N. M. W. Roberts
NERC Isotope Geoscience Laboratory, Nicker Hill, Keyworth, Nottingham NG12 5GG, UK

Introduction

The Rare Earth Elements (REE) play an essential and increasing role in a wide range of consumer electronics, in military applications and in environmental technologies. China currently dominates world production of REE, accounting for over 95 % of current global supply (Hatch 2012). In recent years, China has also imposed export restrictions for REE, leading to global concerns about security of supply (Chakhmouradian and Wall 2012). Consequently, there is considerable interest in identifying new deposits and in understanding the processes responsible for their formation.

Published online: 06 July 2013

Alkaline igneous complexes are an important source of REE, and many such deposits are at an advanced stage of exploration. Rare Earth Element enrichment in these types of deposit can be due to magmatic processes through crystal fractionation or t later magmatic–hydrothermal or hydrothermal activity. Many aspects of the formation of these REE deposits, such as the importance of the role of hydrothermal processes and how and where the parent magmas for these complexes form, are not well understood (Salvi and Williams-Jones 2005; Chakhmouradian and Zaitsev 2012). Investigating the petrology and petrogenesis of these complexes is essential to understand the processes of REE enrichment in these deposit types.

Previous studies by the British Geological Survey (BGS) on Silurian alkaline igneous complexes in north-western Scotland identified elevated REE values (Shaw and Gunn 1993). This suite of igneous complexes is emplaced into the Moine Thrust Zone, at the margin of the Caledonian orogenic belt, and includes the Loch Ailsh and Borralan plutons and Loch Loyal Syenite Complex. These plutons are dominated by syenite, with minor mafic–ultramafic components (Parsons 1999; Goodenough et al. 2011). Rock and stream sediment samples from Loch Borralan, Loch Ailsh and the Loch Loyal Complex indicate relatively high REE contents throughout (Shaw and Gunn 1993). The Loch Ailsh intrusion showed a maximum value of over 7,000 ppm La + Ce in syenite and over 2,000 ppm in pyroxenite. Boreholes from the Loch Borralan pyroxenite showed enrichment in REE with a maximum value of over 2,500 ppm La + Ce. The Cnoc nan Cuilean intrusion of the Loch Loyal Complex showed the greatest values, with the highest recorded value being over 25,000 ppm La + Ce from a heterogeneous basic syenite.

Due to the recent increased global interest in REE, this area was selected for further study, focusing on the Loch Loyal Complex, where the highest values were identified. A short reconnaissance survey on the complex confirmed that the Cnoc nan Cuilean intrusion was of greatest interest. Mapping and 3D modelling of the intrusion (Hughes et al. 2013) have been followed up by geochemical and mineralogical work to investigate the REE mineralisation and the processes responsible for its genesis, and that work is reported in this paper.

Geology of the Loch Loyal Syenite Complex

The Loch Loyal Syenite Complex is situated close to the town of Tongue in northern Scotland, approximately 15 km east of the Moine Thrust Zone, which marks the leading edge of the Caledonian orogenic belt (Fig. 1). It is a part of a suite of Silurian, high Ba-Sr syenitic to granitic plutons which extends across the Northern Highlands, and includes the alkaline igneous complexes within the Moine Thrust Zone (Thompson and Fowler 1986; Fowler et al. 2008). The Loch Loyal Syenite Complex covers an area of about 24 km^2, making it the largest group of alkaline plutons in the British Isles, and comprises three intrusions: Ben Loyal, Beinn Stumanadh and Cnoc nan Cuilean (Fig. 2) (King 1942; Robertson and Parsons 1974). The country rocks to these intrusions are chiefly deformed Neoproterozoic metasedimentary rocks of the Moine Supergroup, with some inliers of Archaean 'Lewisianoid' orthogneisses. Field relationships show that the Loch Loyal Syenite Complex postdates Caledonian deformation in the country rocks (Holdsworth et al. 1999). U–Pb dating of zircon indicates that the complex was emplaced at c. 426 Ma, but efforts to obtain precise dates have been hampered by the abundance of older inherited zircons (Halliday et al. 1987; Goodenough et al. 2011).

The Ben Loyal intrusion is the largest intrusion within the complex, with a surface area of about 16 km^2. It has an approximately semicircular shape truncated to the south-east by the Loch Loyal Fault, a major NE–SW trending dextral oblique fault separating Ben Loyal from the rest of the complex (Holdsworth et al. 2001). The petrography of the whole complex has been described in detail by Robertson and Parsons (1974) and Parsons (1972), and the Ben Loyal intrusion can be subdivided on the basis of mineralogical and textural characteristics. A foliated marginal syenite surrounds a core syenite where foliation is weakly developed or absent (Fig. 2). The core unit is hypersolvus with only one perthitic feldspar present, and the marginal syenite is subsolvus, containing alkali feldspar and albite. The boundary between the two variants is gradational over several hundred metres (Robertson and Parsons 1974; Parsons 1999).

The Beinn Stumanadh intrusion comprises a number of petrographically similar NW–SE-trending sheet-like intrusions which are truncated to the north-west by the Loch Loyal Fault (Holdsworth et al. 2001). The syenite is generally similar to the Ben Loyal marginal syenite, containing two feldspars (Robertson and Parsons 1974).

The Cnoc nan Cuilean intrusion is the most heterogeneous and smallest of the three plutons (King 1942), having a surface area of about 3 km^2. It is also relatively poorly exposed. New mapping of the intrusion (Hughes et al. 2013) has shown that it can be subdivided into two main zones: the Mixed Syenite Zone and the Massive Leucosyenite Zone; Fig. 2). It is dominated by leucosyenite and more mafic melasyenite to monzodiorite, with cross-cutting pegmatite sheets, microgranite veins and biotite–magnetite-rich alteration veins.

The Mixed Syenite Zone occurs on the lower slopes on the eastern and south-eastern sides of Cnoc nan Cuilean (Fig. 2). This zone comprises a mafic syenite to

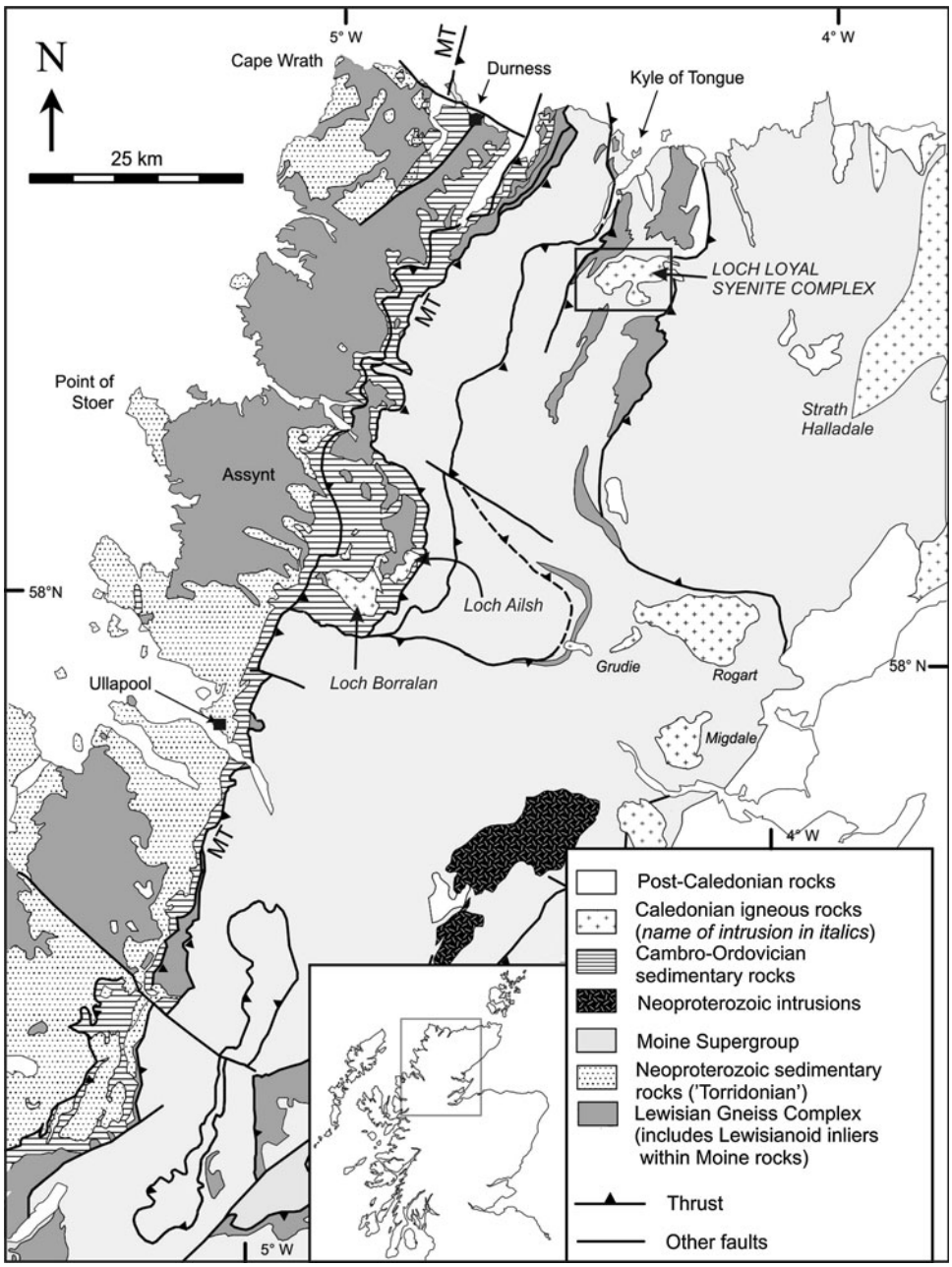

Fig. 1 Geological sketch map of the Northern Highlands of Scotland, indicating the location of some of the major high Ba–Sr intrusions. MT—Moine Thrust, the easternmost and highest thrust in the Moine Thrust Zone. *Box* around the Loch Loyal Syenite Complex shows approximate extent of Fig. 2

monzodiorite phase and a felsic syenite phase, which show complex mixing and mingling textures. The chemical composition of the more mafic phase is highly variable, ranging from syenitic towards monzodioritic; here, we use the term 'melasyenite' as a generic descriptive term for the entire group. Similarly, the term 'leucosyenite' is used for the group of more felsic lithologies. The melasyenite has been partially assimilated by the leucosyenite in some areas, suggesting that both physical and chemical interaction between the two magma phases has occurred (Hughes et al. 2013). Veins of leucosyenite and of later microgranite cut the melasyenite, and xenoliths of country rock are common in this marginal zone. The melasyenite is medium to coarse grained and typically contains more than 30 % mafic minerals, chiefly as clusters of clinopyroxene with some amphibole (Fig. 3a) (Hughes et al. 2013). Titanite, apatite, allanite, and magnetite are common accessories (Fig. 3b).

The Massive Leucosyenite Zone is found in the western area of the intrusion and on topographically higher areas such as the low hills of Meall Eudainn and Creag nan Cat (Fig. 2). This zone is made up of a white to pink massive syenite, locally grading into syenogranite, with less than 10 % melasyenite as enclaves. These lithologies are mineralogically indistinguishable from those in the Mixed Syenite Zone, with the syenites and syenogranites being

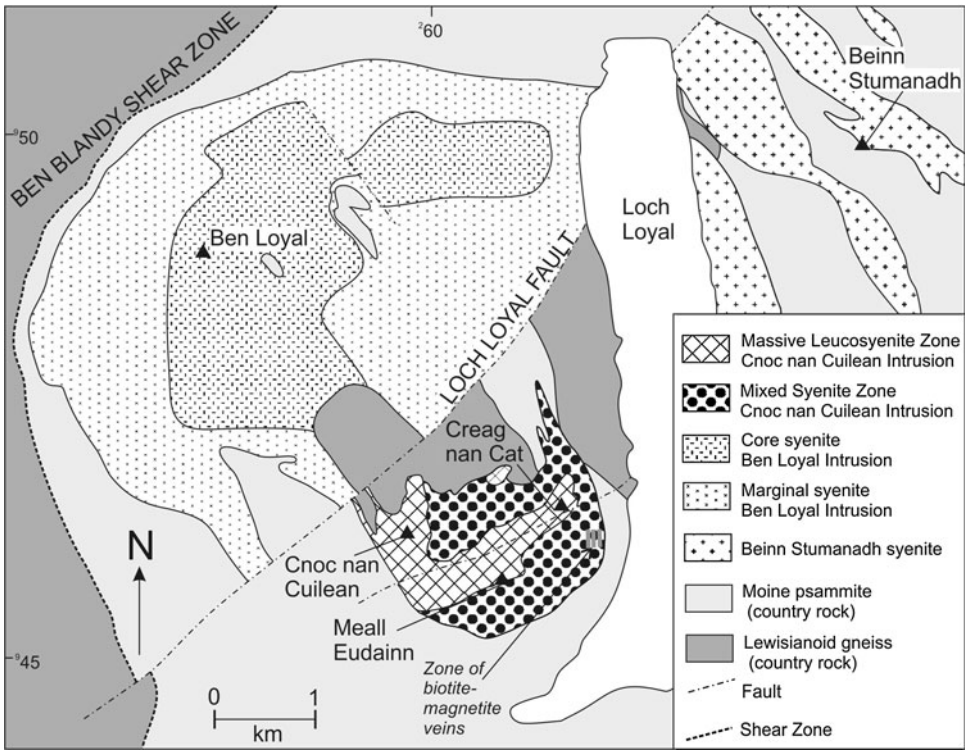

Fig. 2 Geological map of the Loch Loyal Syenite Complex after Robertson and Parsons (1974); Holdsworth et al. (1999); Hughes et al. (2013)

dominated by perthitic K-feldspar with lower modal abundance of plagioclase, 5–15 % quartz and <30 % mafic minerals. The boundary between the two zones is gradational and mapped entirely on the amount of melasyenite lithologies present, with a gradual reduction in melasyenite content over a distance of about 50–100 m. Syenitic pegmatites are present in both the main zones of the intrusion. They occur as irregular patches or sheets usually less than 20 cm wide and are associated with the leucosyenite phase. The term 'leucosyenite' is used as a generic group name for all the more felsic lithologies within the Massive Leucosyenite Zone, including syenites and syenogranites.

Microgranite veins cut all other magmatic phases, including the pegmatites and xenoliths, in both zones of the intrusion (Hughes et al. 2013). The veins are up to a few tens of centimetres wide and are discordant with sharp margins. They are medium grained, equigranular, and comprise roughly equal amounts of plagioclase, K-feldspar and quartz. Mafic minerals are generally absent.

The intrusion has been affected by post-magmatic–hydrothermal alteration, leading to the development of distinctive biotite–magnetite veins. These were identified in one stream section on the eastern side of the intrusion, and the extent of cover by glacial deposits means that their lateral extent is not known. The veins are 30–40 cm thick, steeply dipping, north–south trending and very friable. They crosscut all other lithologies, with the exception of the late microgranite veins. The central parts of these biotite–magnetite veins are considered to represent melasyenite that has been pervasively altered by hydrothermal fluids, grading outwards over tens of centimetres into relatively unaltered syenite and melasyenite (Hughes et al. 2013). The biotite–magnetite veins are very heterogeneous in composition and contain a wide range of minerals, including biotite, magnetite, clinopyroxene, amphibole, K-feldspar, allanite, apatite, barite and rarer accessory minerals such as ancylite, bastnaesite, strontianite and thorite. Biotite is the dominant mineral; it occurs as coarse dark green/brown crystals, as small (<0.5 mm) tabular crystals, and replacing other minerals (Fig. 3c). It is often associated with amphibole.

Magnetite constitutes up to 20 % of these veins; it occurs as both coarse crystals with inclusions of biotite, apatite and allanite, and smaller crystals disseminated throughout the vein, particularly at vein margins (Fig. 3d) (Hughes et al. 2013). Allanite and apatite locally comprise up to 25 and 30 % of the rock, respectively (Fig. 3 e, f), and are described in more detail below. Other trace minerals in the veins include thorite, strontianite and barite. Thorite occurs as inclusions or veinlets within allanite and has caused radial cracking in the host allanite due to radiation damage. Trace amounts of barite and strontianite occur, commonly infilling vugs in magnetite.

Country rock xenoliths, including Moine psammites and semi-pelites and Lewisianoid gneisses, are present in both zones although are more abundant in the Mixed Syenite Zone. They are commonly found in the marginal areas of the intrusion. Some of these are relatively unaltered

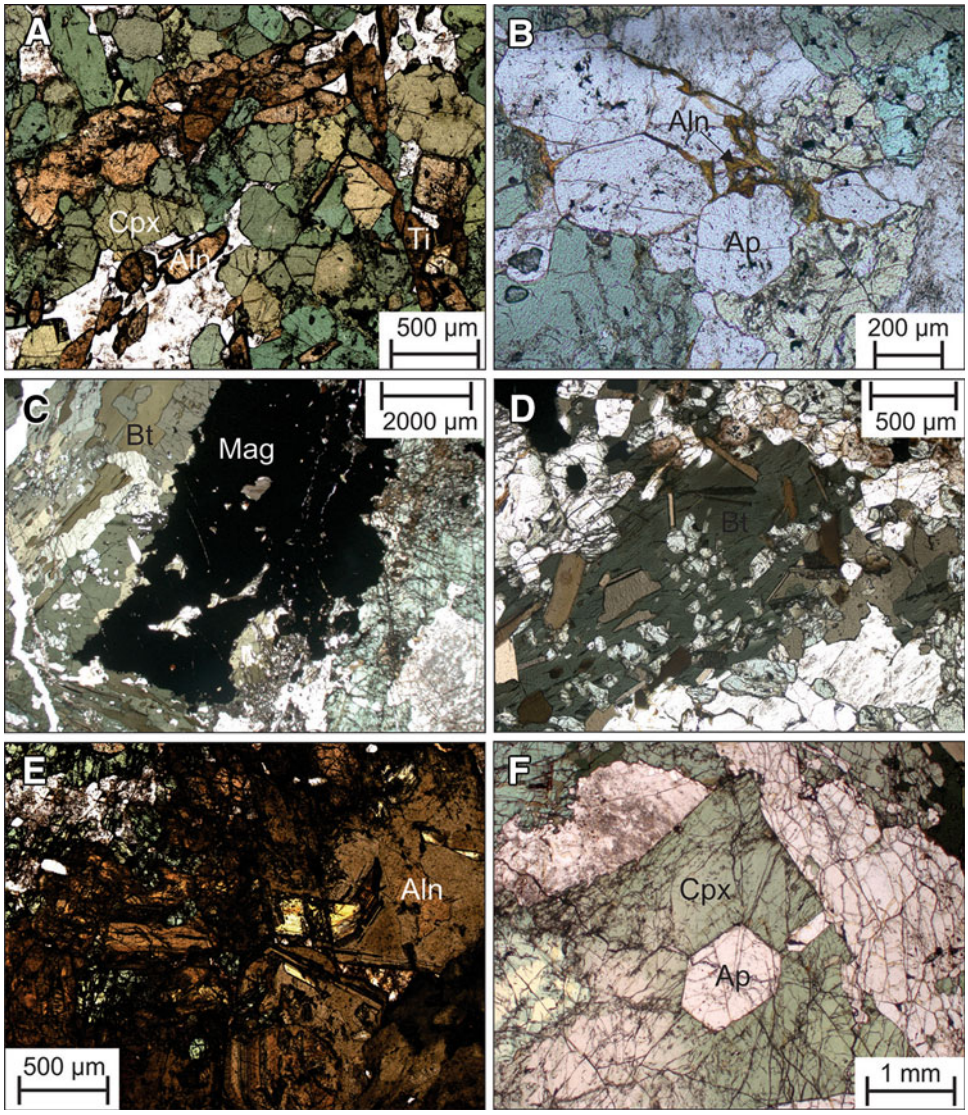

Fig. 3 Photomicrographs of Cnoc nan Cuilean samples. **a** Mafic cluster of clinopyroxene (*Cpx*), titanite (*Ti*) and allanite (*Aln*) (melasyenite sample NWR-009A). **b** *Brownish* allanite rims round apatite (*Ap*) (melasyenite sample NWR-009A). **c** Coarse vuggy magnetite (*Mag*) with apatite and biotite inclusions (biotite–magnetite vein sample NWR-023). **d** Small tabular biotite (*Bt*) crystals intergrown with coarse *dark green* biotite (biotite–magnetite vein sample NWR-023). **e** Coarse, *dark brown* zoned allanite with *yellow* alteration (biotite–magnetite vein sample HH18). **f** Coarse euhedral apatite in clinopyroxene (biotite–magnetite vein sample NWR-023)

although others show evidence of partial assimilation, or alteration similar to that in the biotite–magnetite veins.

Occurrence of REE-bearing minerals at Cnoc nan Cuilean

Allanite

Allanite is the main REE-bearing mineral in the Cnoc nan Cuilean intrusion, being present in all major lithologies. It is most dominant in the biotite–magnetite veins, where it comprises up to 25 % of the rock, and is more abundant in the melasyenite (1–7 %) than in the leucosyenite (<1 %). Petrographic evidence suggests that there are three main generations of allanite in the Cnoc nan Cuilean intrusion: (1) late-magmatic allanite found in all the syenites and in the biotite–magnetite veins; (2) post-magmatic–hydrothermal allanite veinlets also found in all the lithologies; and (3) post-magmatic, large allanite crystals found only in the biotite–magnetite veins.

The late-magmatic allanite is present in all syenite lithologies, although predominantly in the melasyenite. It is generally anhedral to subhedral, dark brown to reddish brown and strongly pleochroic. It is present as narrow rims around apatite or as blocky crystals interstitial to minerals such as clinopyroxene, titanite and apatite and is therefore thought to have formed late in the crystallisation sequence (Fig. 4a, b).

Narrow allanite veinlets ranging from <1 to about 4 mm wide occur in all syenite types although predominantly in the melasyenite (Fig. 4c). These veinlets cut all other mineral phases, so must have formed after crystallisation of the host syenite, but are crosscut and offset by the later microgranite veins.

The third generation of allanite is found only in the biotite–magnetite veins. Crystals are coarse (up to ~5 mm) and

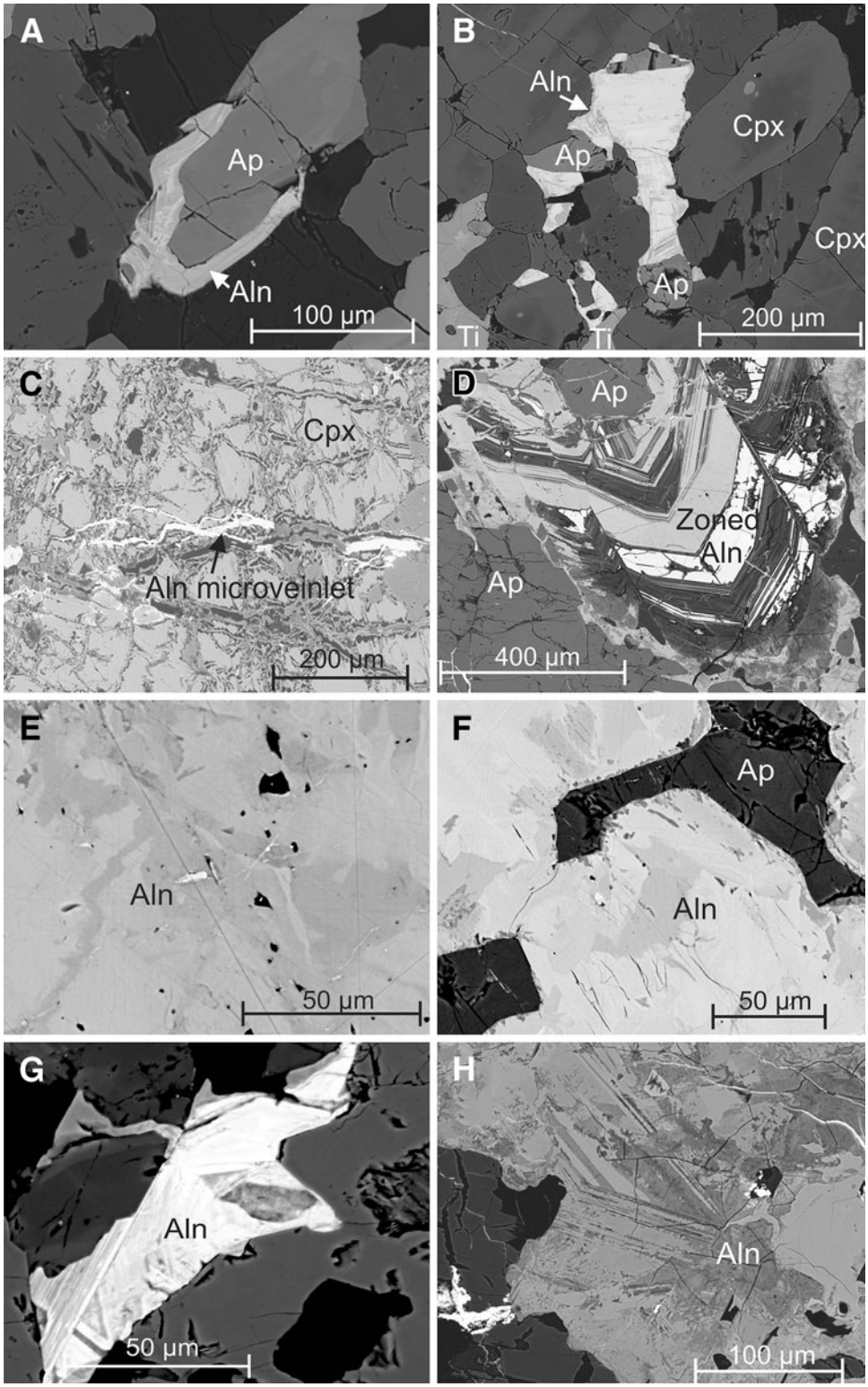

Fig. 4 BSE images of allanite. **a** Late-magmatic allanite (*Aln*) rim around apatite (*Ap*) (melasyenite sample HH6). **b** Late-magmatic allanite interstitial to apatite, clinopyroxene (*Cpx*) and titanite (*Ti*) (melasyenite sample HH6). **c** Allanite micro-veinlet cutting melasyenite (leucosyenite sample HH12). **d** Euhedral, zoned allanite showing alteration preferentially along growth zones (biotite–magnetite vein sample HH18). **e** Massive allanite showing irregular patchy alteration (biotite–magnetite vein sample HH18). **f** Massive allanite with alteration selvage at the apatite/allanite boundary (biotite–magnetite vein sample HH18). **g** Late-magmatic allanite with *dark* core and alteration preferentially along growth zoning (melasyenite sample HH15). **h** Massive allanite replacing zoned allanite (biotite–magnetite vein sample HH21)

vary in colour from dark red-brown to yellow (Fig. 3e). Use of a scanning electron microscope (SEM) under back-scattered electron (BSE) imaging conditions shows that some allanite in these veins occurs as euhedral crystals with complex growth zoning (Fig. 4d), whereas other crystals have massive internal textures with some irregular, patchy zoning and common inclusions of magnetite and apatite (Fig. 4e).

Allanite has been shown to be prone to hydrothermal alteration (Morin 1977; Wood and Ricketts 2000; Poitrasson 2002),

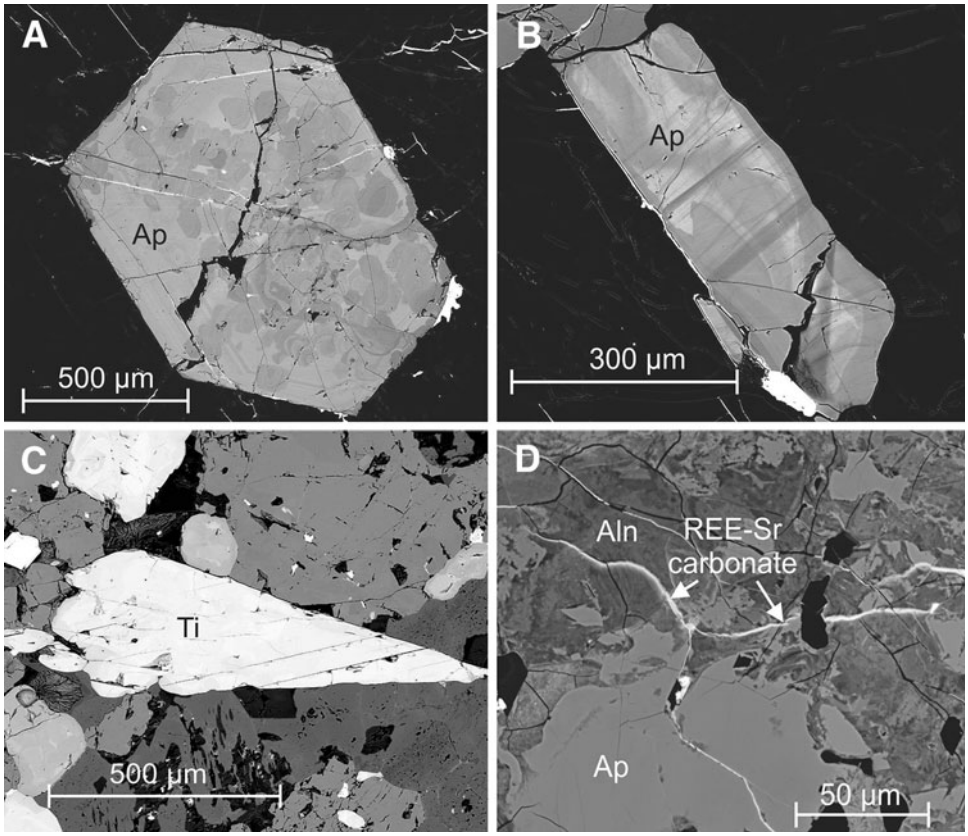

Fig. 5 BSEM images of other REE-bearing minerals. **a** Euhedral zoned apatite (*Ap*) with inclusions of earlier apatite (biotite–magnetite vein sample NWR-023). **b** Zoned apatite showing suture lines from annealed cracks (biotite–magnetite vein sample NWR-023). **c** Euhedral titanite crystal showing faint zoning on the *left hand side* (melasyenite sample HH15). **d** Cross-cutting REE–Sr carbonate veinlets cutting allanite and apatite (biotite–magnetite vein sample biotite–magnetite vein sample HH21)

and all allanite generations in the Cnoc nan Cuilean samples show evidence of alteration, particularly the biotite–magnetite vein allanite. Altered areas appear yellow in thin section and are verging on isotropic (Fig. 3e). These altered areas generally appear darker in BSE imagery, suggesting that the mean atomic number has decreased; this is consistent with the incorporation of water during alteration (Ghent 1972). The pattern of alteration varies; it can appear as patchy 'halos' near fractures with irregular limits (Fig. 4e, f), or preferentially along some original growth zones parallel to crystal margins (Fig. 4d). The latter type of alteration along zoning is more common in the coarse biotite–magnetite vein allanite, but is also seen in the late-magmatic allanite in melasyenite samples (Fig. 4g). In the biotite–magnetite veins, extensive hydrothermal alteration has locally destroyed the zoning entirely (Fig. 4h).

Apatite

Apatite is present in all magmatic lithologies and in the biotite–magnetite veins and represents a likely secondary host for the REE. Similarly to allanite, it is most abundant in the biotite–magnetite veins (10–30 %). Melasyenite generally contains 2–10 % apatite, whereas leucosyenite has <1 %. Apatite commonly occurs as euhedral grains associated with clinopyroxene and titanite, with common allanite rims. A second stage of apatite formation can be recognised in the biotite–magnetite veins, where clusters of earlier apatite are enclosed within larger zoned apatite crystals. Some of these appear to have been resorbed into the later apatite leaving internal crystal outline textures (Fig. 5a). Back-scattered electron images show that some crystals contain annealed fractures (Fig. 5b). Apatite grains commonly occur at the core of zoned allanite crystals or as inclusions within allanite.

Titanite

Titanite is common in all syenite lithologies, making up 1–5 % of the leucosyenite and 2–7 % of the melasyenite. It generally occurs as euhedral, rhombic crystals, commonly in mafic clusters with clinopyroxene, apatite and allanite (Fig. 3a). Grain size varies between about 50 µm and 1 mm, and larger crystals show faint zoning (Fig. 5c). In the biotite–magnetite veins, titanite is generally only present in trace amounts as inclusions within mafic minerals or in clusters associated with clinopyroxene and amphibole.

Other REE-bearing minerals

An unidentified Sr-enriched REE-carbonate forms bifurcating veinlets up to about 50 µm thick that crosscut all mineral phases within the biotite–magnetite veins,

indicating that this is the last REE-bearing phase to form (Fig. 5d). This mineral also infills vugs within the biotite–magnetite veins.

Analytical techniques

Mineral chemistry

Quantitative microanalysis was carried out on minerals from on a range of melasyenite and biotite–magnetite vein samples. A total of 465 analyses were obtained, but many of these were from areas that have been affected by alteration and metamictisation. Allanite was the focus of this analysis, particularly the late-magmatic and biotite–magnetite vein phases, but other REE-bearing minerals, such as apatite, titanite and REE carbonates, were also analysed.

These minerals were analysed at the British Geological Survey petrography and microanalysis facility laboratories. Polished thin sections were carbon coated to a thickness of 25 nm using an EMITECH 960L evaporation-coating unit. Quantitative microanalysis of the samples was performed using an FEI QUANTA 600 environmental scanning electron microscope (SEM), fitted with an Oxford Instruments X-MAX large area (50 mm^2) silicon drift detector (SDD) energy-dispersive X-ray microanalysis (EDXA) system, run with Oxford Instruments' INCA (v.4) software. SEM-based analysis was particularly suited to the complex and very fine nature of the mineral textures and compositional variations seen within these samples, and to the need for clear imaging of the textures.

For microanalysis, the SEM operated under conditions of high vacuum ($<1.2 \times 10^{-4}$ Torr), using an accelerating voltage of 20 kV, at the instruments' optimal analytical working distance of 10.00 mm with a detector take-off angle of 45°. Beam current conditions were customised to take account of the beam sensitivity of various analysed mineral phases; altered allanite and carbonates in particular were expected to be sensitive and were exposed to lower beam current. On the FEI Quanta 600, beam current is controlled by spot size on a scale of 1–10; values between 6.0 and 7.4 were used, equating to Faraday cup measured currents of 2–10 nA. Analytical livetimes of 30–60 s were used for spot and small area (<5 µm across) raster analyses. Area raster analyses were again used where mineral beam sensitivity was considered to be a factor. EDXA detector noise reduction process time was set to optimise for the instrument conditions, detector type and elemental compositions of the mineral phases being analysed (INCA software 'Process time' setting 4). INCA software applies "phi-rho-z" matrix correction methods (after Pouchou et al. (1990)) and uses multiple least squares for peak deconvolution.

The SEM used for quantitative microanalysis has been calibrated using a combination of pure element and mineral standards. These calibrations have been checked against and found to be in excellent agreement with BGS standards (cross-checked against other beam instruments), National Institute of Standards and Technology (NIST) samples (e.g. NIST610, 612; compositions taken from Jochum et al. (2011)) and also manufactured REE standards (Drake and Weill 1972). These show that for major elements in a silicate matrix, bias is less than 5 % and precision (at 2 × SD) better than 6 % (and better than 2 % where the element concentration is >10 wt%). Specifically for the REE, in silicate matrix materials with 3–4 wt% of various REE groupings, bias is typically less than 5 % with some exceptions (e.g. Nd and Y at around 10 %), and precision is better than 6 %. These are consistent with the findings outlined in the ASTM Standard-E1508 (2012a) guide for quantitative EDXA, which indicate that the methodology produces comparable quality results to conventional WDXA major element analysis.

Procedures used for the SEM-EDXA quantitative microanalysis were in line with those recommended by the ASTM Standard (ASTM Standard-E1508 2012a). Prior to analysis, beam stability was established by initial monitoring of specimen current over an extended period (>30 min) whilst in spot mode on a Co primary standard. As final confirmation of stability, three consecutive analyses run on the Co primary standard were required to return totals within a <1 % range before proceeding. During collection of microanalysis data, repeat Co standard calibrations were performed every 20 min to monitor and correct for beam drift.

The formula of allanite was calculated on the basis of 12.5 oxygen atoms. Representative analyses of allanite and other REE-bearing minerals are given in Table 1; a fuller version of the dataset is reported in tables A and B in the electronic annex.

U–Pb geochronology

U–Pb geochronology was conducted on titanite and allanite using a laser ablation inductively coupled mass spectrometer system (LA-ICP-MS) at the NERC Isotope Geosciences Laboratory, Nottingham. A New Wave Research UP193ss laser ablation system was utilised along with a Nu Instruments Attom HR-ICP-MS. The method for titanite analysis is reported in Thomas et al. (2013), and the method for allanite is the same as that for monazite, as reported in Palin et al. (2013). In brief, ablation consisted of a 30 s ablation using 35 µm spots, a fluence of ~2.5 J/cm^2, with a washout of 10 s. $^{207}Pb/^{206}Pb$ and $^{206}Pb/^{238}U$ ratios were normalised to matrix-matched reference materials; the precision and

Table 1 Representative quantitative analyses of allanite and other REE-bearing minerals

Sample Mineral	HH6 Late-magmatic allanite	HH32 Late-magmatic allanite	HH17 Micro-veinlet allanite	NWR-023 Bt-mag vein allanite	HH18 Bt-mag vein allanite	NWR-023 Bt-mag vein apatite	HH_6 Mela-syenite apatite	HH_15 Mela-syenite titanite
SiO_2 (wt%)	32.1	34.6	34.8	31.4	38.9	1.4	1.2	30.3
Al_2O_3 (wt%)	12.6	16.7	11.3	12.0	15.9	0.1	0.1	1.6
CaO (wt%)	10.9	15.0	8.9	11.3	7.5	52.7	52.6	25.6
Fe as Fe_2O_3 (wt%)	13.5	15.2	14.2	16.3	7.3	0.1	0.0	2.3
MnO (wt%)	0.5	0.0	0.7	0.3	0.4	n.d.	n.d.	n.d.
MgO (wt%)	0.9	0.0	0.3	1.0	0.0	n.d.	n.d.	n.d.
TiO_2 (wt%)	0.9	0.3	1.0	1.3	0.8	0.1	0.0	31.1
SrO (wt%)	0.8	1.1	0.8	0.5	1.0	1.5	1.6	n.d.
Na_2O (wt%)	0.4	0.0	0.0	0.0	0.0	0.2	0.0	n.d.
P_2O_5 (wt%)	n.d.	n.d.	n.d.	n.d.	n.d.	40.5	41.4	n.d.
Y_2O_3 (wt%)	0.4	0.0	0.0	0.5	0.0	0.0	0.0	0.9
La_20_3 (wt%)	7.2	2.0	5.1	7.0	6.3	0.4	0.4	0.6
Ce_2O_3 (wt%)	11.7	7.0	11.5	11.1	11.1	0.5	0.5	0.8
Pr_2O_3 (wt%)	0.9	1.0	1.1	0.9	0.9	0.0	0.0	n.d.
Nd_2O_3 (wt%)	2.8	4.0	3.6	3.1	3.4	1.1	0.9	1.6
Sm_2O_3 (wt%)	0.2	0.6	0.0	0.2	0.0	0.2	0.2	n.d.
Eu_2O_3 (wt%)	0.0	0.0	0.0	0.0	0.0	0.0	0.0	n.d.
Gd_2O_3 (wt%)	1.0	0.0	0.0	1.1	0.0	0.0	0.0	n.d.
Dy_2O_3 (wt%)	n.d.	n.d.	n.d.	n.d.	n.d.	n.d.	n.d.	n.d.
ThO_2 (wt%)	1.0	0.5	1.4	0.7	2.1	0.3	0.0	0.5
F (wt%)	0.0	0.0	0.0	0.0	0.0	0.0	0.0	0.0
Cl (wt%)	0.1	0.0	0.1	0.0	0.0	0.0	0.0	0.0
Total (wt%)	98.0	98.3	96.5	98.9	98.3	100.1	99.7	96.2
TREO (wt%)	23.8	14.6	21.4	23.4	21.7	2.2	1.9	3.0

$FeO + Fe_2O_3$ have not been apportioned due to alteration of the minerals and low analytical totals

accuracy achieved were both 2–3 %. Allanite was normalised to an in-house material (40010; Roberts et al. (2012)), and Tara was used as a secondary reference material to check on precision and accuracy and produced an age of 414 ± 15 (accepted age 415 ± 3 Ma; Gregory et al. (2007)). Titanite was normalised to Ontario2 (Spencer et al. 2013), and Fish Canyon Tuff titanite was used as a secondary reference material; the age obtained was 29.5 ± 1.2 Ma (accepted age 28.4 ± 0.05 Ma; Schmitz and Bowring (2001)).

Whole rock geochemistry

Samples were crushed, subsampled and milled using an agate ball mill. Major element oxide concentrations were determined by X-ray fluorescence spectroscopy (XRF) and trace and REE by inductively coupled plasma mass spectrometry (ICP-MS) at the British Geological Survey (BGS). Samples for ICP-MS underwent 'total' dissolution using a sodium peroxide fusion, followed by a mixed acid dissolution. Samples for XRF were dried at 105 °C and

then heated to 1,050 °C for an hour before loss on ignition was determined. Fused beads were produced by fusion at 1,200 °C.

Uncertainty budgets (expanded uncertainty with a coverage factor of 2, representing the 95 % confidence interval) have been calculated for XRF fused bead work during the method validation before UKAS accreditation of the laboratories at BGS (now PANalytical Nottingham). Estimates of the absolute uncertainty, at analyte concentrations at least an order of magnitude greater than the reporting limit, are from 0.1 to 1 % for the major elements. Routine chemical quality control solutions demonstrate typical long-term precision of analyses better than 10 % relative standard deviation (RSD) for most elements by ICP-MS. Analyses of a wide variety of reference materials demonstrate typical long-term precision of analyses better than 15 % RSD for most elements; this assumes that they are significantly higher than detection limits.

Mineral chemistry of REE-bearing minerals at Cnoc nan Cuilean

Allanite and alteration products

Allanite was analysed from three melasyenite samples, three biotite–magnetite vein samples and one sample from the contact of the biotite–magnetite vein. All of the analysed crystals are allanite-(Ce) with the general formula $(Ca, Ce, La, Nd, Y)_2$ $(Al, Fe^{2+}, Fe^{3+}, Ti)_3$ $(SiO_4)_3$ (OH) and are Light Rare Earth Element (LREE) dominated (Table 1). Late-magmatic allanite was analysed from all three melasyenite samples, but the allanite micro-veinlets are a relatively minor constituent and were only analysed in one sample of melasyenite. Post-magmatic biotite–magnetite vein allanite was analysed from four samples within and at the contact of a vein. Data for representative samples are given in Table 1, and a wider dataset is presented in Table A in the electronic annex.

The late-magmatic allanite has relatively consistent Total Rare Earth Oxide (TREO) values (13–25 wt%), and the micro-veinlet allanite shows similar concentrations (19–23 wt%). TREO concentrations for the biotite–magnetite vein allanite vary more widely, from 9 to 52 wt%, although allanite with the more extreme TREO contents typically shows very poor analytical totals. This wide range is probably a consequence of original growth compositional variations combined with the extensive and varied degree of alteration. REO distributions show that all the allanite is Ce dominated (averaging 50–52 % of the TREO across all samples). La contents are lower and more variable (averaging 29 % in the biotite–magnetite veins and 25 % in the late-magmatic allanite) as are Nd contents (averaging 14 and 17 %, respectively). Y and the HREO are rarely detectable.

TREO and TiO_2 in the full allanite dataset have a very weak positive correlation (correlation coefficient 0.18), indicating the likelihood of different controls on their behaviour. Al_2O_3 content shows a moderate negative correlation (correlation coefficient 0.68) with TREO content (Fig. 6a, b); this is typical, as increasing REE contents are typically associated with replacement of Al by ferrous iron to balance the charge of the REE (Petrik et al. 1995). These trends are more pronounced in the late-magmatic and micro-veinlet allanites, but are also seen in allanite from the biotite–magnetite veins.

Allanite compositions expressed in terms of aluminium and total REE + Y + Th + Sr + Mn contents are projected in the diagram of Petrik et al. (1995) (Fig. 6c), and all plot within the allanite-ferriallanite field. Many of the compositions, mainly in the more extensively altered grains, yield TREE + Y + Th + Sr + Mn > 1.2 and have not been included on this plot. This diagram shows that the allanite types have slight compositional differences. The allanite micro-veinlets are compositionally very similar to the late-magmatic allanite, but lie at the higher end of total TREE + Y + Th + Sr + Mn. The biotite–magnetite vein allanite varies considerably but in general tends towards higher Al^{3+} and TREE + Y + Th + Mn + Sr contents than the late-magmatic allanite. The allanite analyses from the sample at the contact between the melasyenite and biotite–magnetite vein tend to plot further to the left of the diagram with lower Al^{3+} but a similar range of TREE + Y + Th + Mn + Sr. In general, the Cnoc nan Cuilean allanites plot in the area expected for allanites in igneous rocks in extensional or anorogenic settings, rather than that expected in areas of compressive tectonics (Vlach and Gualda 2007).

As discussed earlier, the most altered areas in allanite crystals generally appear darker grey in BSE imagery. Quantitative analysis shows that these altered areas have low analytical totals, probably due to the incorporation of volatiles such as water during the alteration process (Ghent 1972). Altered areas are typically characterised by higher Sr, Ti, Mn and Th contents but lower REE, Al, Ca and Si contents than the unaltered allanite. An exception to this is represented by certain zones of allanite in the biotite–magnetite veins, which are characterised by high BSE brightness and low analytical totals but considerable REE enrichments. They are also depleted in Ca, Al, Si, as are other altered areas and show relatively high Th and Sr levels, but are not enriched in Ti or Mn.

Both these alteration characteristics are clearly shown in one biotite–magnetite vein sample (HH18) where alteration has occurred preferentially along the original growth zones.

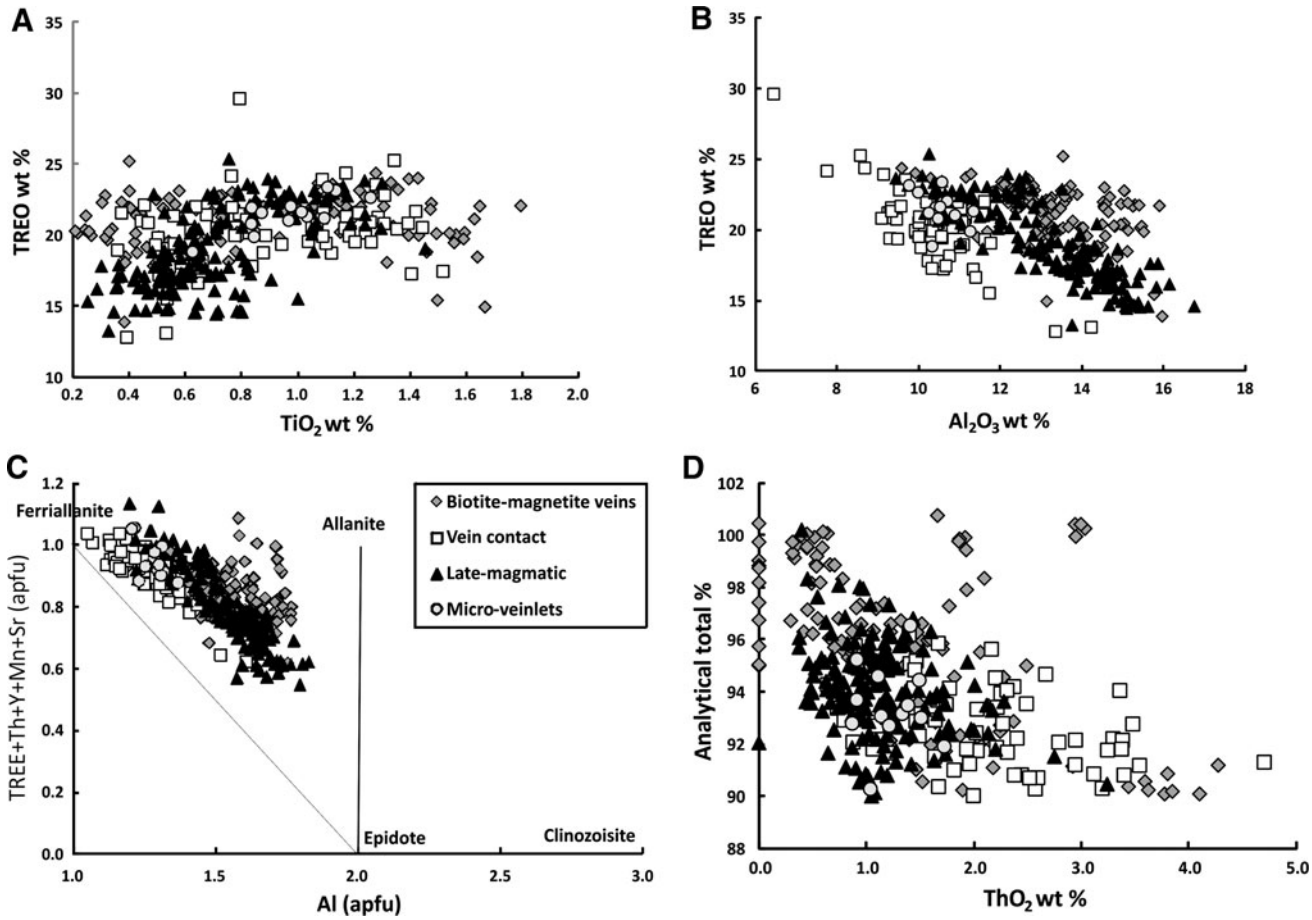

Fig. 6 Compositional diagrams for allanite. **a** TiO_2 versus TREO relations of allanites. **b** Al_2O_3 versus TREO relations of allanites. **c** All allanite analyses plotted on the diagram of Petrik et al. (1995) showing Al versus TREE + Y + Th + Mn + Sr. **d** Analytical totals versus ThO_2 relations of allanite

SEM-EDXA-derived element mapping clearly shows the compositional differences between each zone (Fig. 7). A dark, highly altered zone recognised in BSE imagery is depleted in Al, Si and REE and is Th-rich. In contrast, a high brightness zone is clearly REE enriched; quantitative analyses in this zone show up to 38.6 % TREO. Nd, F and Sr have not been included on this element map due to interference from other elements.

Alteration features emphasise original characteristics, for example, growth zones—it appears that more Th-rich bands have been altered to a greater extent than those less Th-rich. The extent of the alteration may be due to metamictisation and destruction of the crystal structure, due to bombardment by alpha particles that result from the decay of radioactive elements such as Th in the mineral. This lowered stability makes the mineral more susceptible to alteration (Deer et al. 1992). The analyses show a moderately developed negative correlation between analytical total and Th content, providing further evidence that increased degree of alteration is linked to thorium content (Fig. 6d).

Other REE-bearing minerals

Apatite

Apatite from the biotite–magnetite veins on average contains slightly higher TREO values than that from the melasyenite, though the differences are small. Distribution of REE within the vein and melasyenite apatites is very similar (Table B of ESM). Both are Nd dominated (44 % of the REE on average) followed by Ce and La (30 and 18 %, respectively) and no detectable Y or HREO. Fluorine contents are high, although quantitative values are not obtained from the SEM; apatite from both the melasyenite and the biotite–magnetite veins is actually fluorapatite. All grains analysed are also relatively Sr-rich with values up to 1.9 wt%. Th is rarely detectable, with a maximum value of 0.6 wt%.

Titanite

Some titanite was analysed from one of the melasyenite samples (Table B of ESM). TREO values range from

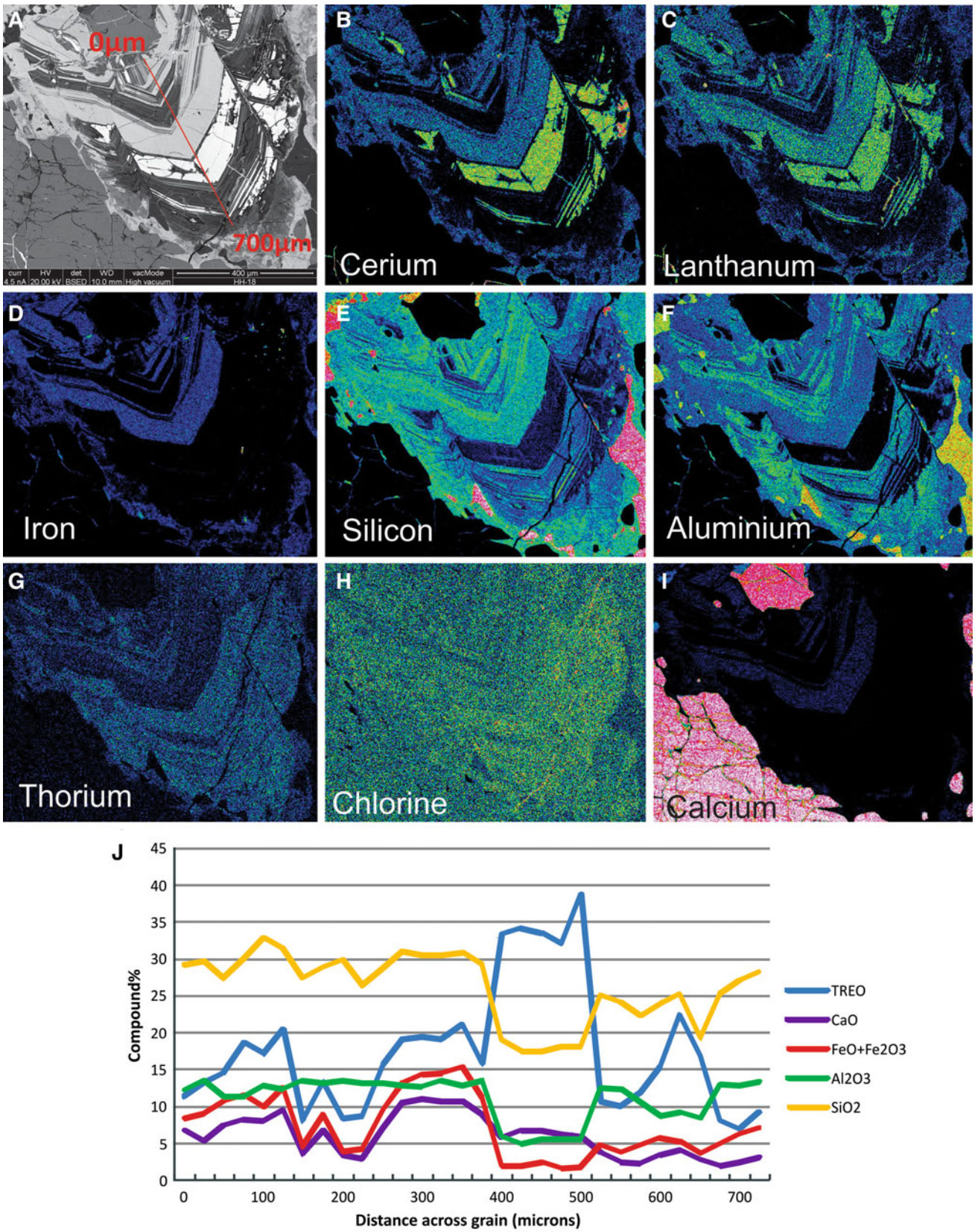

Fig. 7 SEM-EDX element maps and linescan data for a zoned allanite grain from a biotite–magnetite vein sample (HH18). **a** BSE image showing linescan. **b** Cerium. **c** Lanthanum. **d** Iron. **e** Silicon. **f** Aluminium. **g** Thorium. **h** Chlorine. **i** Calcium. **j** Graph showing element variation across grain

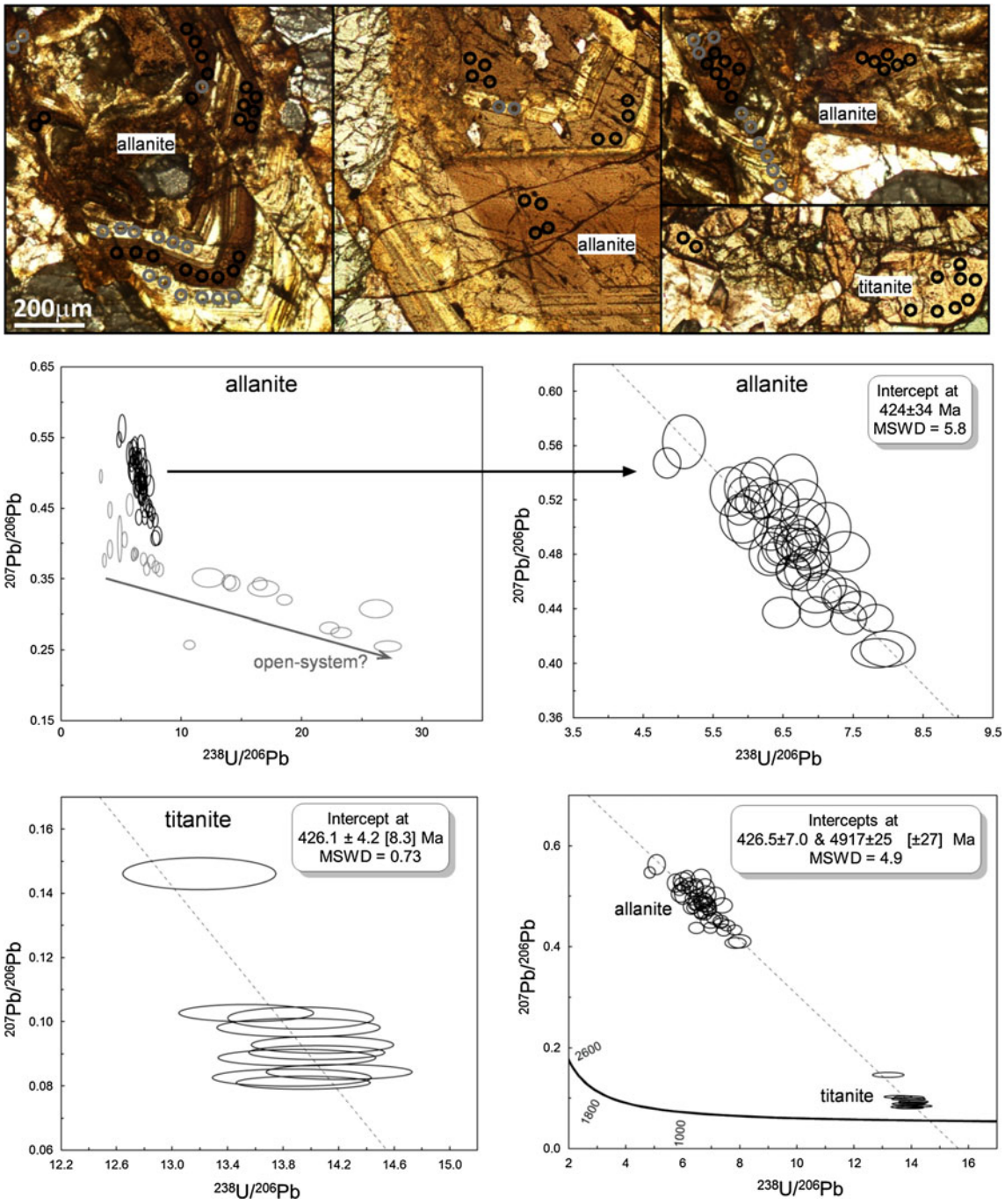

Fig. 8 Dated allanite and titanite crystals with ablation spots indicated (all at *same scale*), and Tera-Wasserburg plots of U–Pb results. *Black* and *grey spots/ellipses* correlate broadly with *dark* and *bright* allanite zones, respectively. All *ellipses* are plotted and uncertainties given at 2σ

3.01 to 4.91 wt%, and they are Ce and Nd dominant with these elements making up an average of 43 and 40 %, respectively, of the total REE. Unlike the other REE-bearing minerals, Y is detectable in some analyses, up to 0.93 wt%.

REE carbonates

The REE-carbonate veins show the highest TREO contents of all REE-bearing minerals in the Cnoc nan Cuilean intrusion, with up to 68.35 wt% TREO. The REE-Sr

carbonate veins have lower contents with an average of 44.63 wt% TREO. Both show similar REO distributions to the allanite, being Ce dominated (48–50 %), with 29–31 wt% La and 13–15 wt% Nd. The REE-Sr carbonate veins show detectable Y and HREO with maximum values of 0.68 wt% Y and 2.83 wt% Gd.

U–Pb geochronology of allanite and titanite, Cnoc nan Cuilean

Allanite and titanite from a biotite–magnetite vein sample (HH18) were selected for U–Pb geochronology. The analysed allanite forms a large crystal with complex growth zoning (Fig. 4d). As described above, this allanite contains zones that are near-isotropic in thin section and appear dark in BSE imagery; quantitative analysis has shown that these zones are highly altered and are REE depleted. The same crystal also contains zones that appear very bright in BSE imagery; these are also highly altered, but are REE enriched.

Both dark and bright zones were analysed (Fig. 8), and both had high common lead contents (Table C, electronic annex). The dark allanite, when anchored to an estimated common lead composition based on Stacey and Kramers (1975), gives a poor regression (MSWD = 5.8) to a lower intercept of 424 ± 34 Ma. The bright allanite partly overlaps this regression, but has a much greater spread, and ranges to higher U/Pb ratios; this is interpreted as open-system disturbance of the U–Pb systematics in these parts of the allanite mineralisation.

Titanite has much lower common lead content that the allanite, giving an overlapping but more robust age of 426.1 ± 8.3 Ma (MSWD = 0.73). A regression through both allanite and titanite gives an equivalent age of 426.5 ± 7 Ma (MSWD = 4.9), indicating that the estimated common lead compositions are accurate. Both allanite and titanite crystallised at c. 426 Ma, which overlaps with the previous estimate of pluton crystallisation based on zircon ages (Halliday et al. 1987). However, the difficulty of obtaining high-precision ages from these altered lithologies means that it is not possible to separate out the different events recognised on the basis of petrography.

Whole rock geochemistry of the Loch Loyal syenites

Major elements

Twenty-eight samples from all parts of the Loch Loyal Syenite Complex were analysed for major elements by XRF, with the majority of samples from the Cnoc nan Cuilean intrusion. There is considerable major element variation between the different lithologies within the Cnoc nan Cuilean intrusion, compared to the relatively homogenous Ben Loyal and Beinn Stumanadh syenites (Table 2; Fig. 9). The compositions of the Ben Loyal, Beinn Stumanadh and Cnoc nan Cuilean leucosyenite predominantly lie in the syenite field of the total alkali-silica diagram (Fig. 9) with the Cnoc nan Cuilean melasyenite group varying in composition from monzodiorite to syenite. The compositions of the leucosyenite range from 63–76 % SiO_2 and 9–12 % $Na_2O + K_2O$. The melasyenite contains less silica, ranging from 49–65 %, and has a broader range of $Na_2O + K_2O$ values (4–12 %). This is consistent with field and petrological observations which show the Ben Loyal and Beinn Stumanadh intrusions to be relatively homogenous and Cnoc nan Cuilean to be highly heterogeneous. The biotite–magnetite veins are too highly altered to be classified using this diagram.

Major element variation diagrams show extensive element arrays for the Cnoc nan Cuilean lithologies, but again, the Ben Loyal and Beinn Stumanadh syenites are relatively homogeneous (Fig. 10). MgO, CaO and Fe_2O_3 levels decrease as silica increases which is consistent with progressive removal of mafic minerals such as clinopyroxene and amphibole from a mantle-derived parent magma. P_2O_5 shows a similar relationship with silica suggesting progressive removal of apatite from the melt. Levels of Na_2O, K_2O and Al_2O_3 increase with silica although K_2O and Al_2O_3 show inflections at about 60 % silica, presumably indicating the onset of K-feldspar fractionation.

Trace elements

A larger suite of 42 samples was analysed for trace elements and REE by ICP-MS. Trace element variations within the Cnoc nan Cuilean lithologies are extensive, but again, the Ben Loyal and Beinn Stumanadh syenites are relatively homogeneous (Table 3; Fig. 11). All lithologies have high concentrations of Ba, Sr and the LREE and low levels of Nb, Ta and the heavy REE (HREE). These characteristics support their classification as part of the high Ba–Sr igneous suite by published work (Tarney and Jones 1994; Fowler et al. 2008). The melasyenite shows the highest Ba and Sr contents with averages of 8,887 and 3,036 ppm, respectively, and ranges of 1,692–24,765 ppm and 1,259–5,866 ppm.

Multi-element normalised diagrams for all Loch Loyal lithologies are shown in Fig. 11. Although the overall element concentrations differ greatly, the syenites share similar patterns, suggesting that the magmas were derived from a common source region. All patterns show common features such as distinct Nb, Ti and P troughs and enrichment in Th, Ba, Sr and the LREE. The negative Nb–Ta

Table 2 Whole rock major element data for all Loch Loyal Syenite Complex lithologies

	Easting	Northing	SiO_2 (wt%)	TiO_2 (wt%)	Al_2O_3 (wt%)	Fe_2O_3 (wt%)	MnO (wt%)	MgO (wt%)	CaO (wt%)	Na_2O (wt%)	K_2O (wt%)	P_2O_5 (wt%)	LOI (wt%)	Total (wt%)
Ben Loyal														
NWR-005	261243	949734	65.32	0.36	16.54	2.60	0.06	0.86	1.21	5.97	5.55	0.23	0.41	99.82
NWR-006	260980	949747	65.53	0.34	16.17	2.46	0.06	0.86	1.60	5.82	5.47	0.22	0.42	99.68
Beinn Stumanadh														
NWR-012	262911	950748	65.84	0.30	16.58	2.11	0.07	0.27	1.01	5.57	5.94	0.21	1.24	99.83
NWR-013	262780	950753	65.12	0.26	16.90	2.00	0.08	0.22	0.97	5.81	5.94	0.18	1.20	99.56
NWR-014	262702	950718	66.04	0.27	16.88	2.03	0.06	0.17	0.89	5.71	5.94	0.15	0.93	99.79
NWR-015	262829	950355	65.89	0.29	16.79	2.05	0.08	0.47	0.84	5.46	6.24	0.20	1.04	100.11
NWR-016	263691	949603	76.12	0.42	11.20	2.80	0.06	0.51	0.55	2.86	4.00	0.06	1.02	99.90
NWR-018	264125	949893	69.47	0.27	15.11	2.24	0.04	0.32	0.41	4.49	6.20	0.19	0.62	99.95
NWR-019	262845	949123	65.61	0.31	16.01	2.46	0.09	0.50	1.22	5.78	5.58	0.29	0.67	99.34
Cnoc nan Cuilean leucosyenite														
NWR-009	261532	946076	63.99	0.33	14.96	3.71	0.09	1.29	2.76	3.96	6.71	0.41	0.62	99.86
NWR-027	260012	946062	72.35	0.11	14.65	1.27	0.03	0.23	0.59	5.27	4.78	0.06	0.29	100.08
NWR-030	259907	946170	75.33	0.04	13.65	0.57	0.01	0.03	0.16	5.34	4.03	0.01	0.59	99.88
HH_8	259731	946197	61.37	0.48	15.35	3.53	0.09	1.50	4.04	5.16	6.27	0.33	0.47	99.48
Cnoc nan Cuilean melasyenite														
NWR-009A	261532	946076	50.52	0.36	8.64	9.37	0.38	4.77	14.77	2.67	3.29	2.87	0.23	99.22
NWR-020	261633	946074	59.64	0.33	16.37	3.36	0.09	1.76	3.91	4.03	7.32	0.65	0.54	99.86
NWR-021	261593	946049	55.87	0.34	13.73	4.35	0.14	0.32	7.05	0.93	8.71	0.75	6.02	99.68
NWR-022	261597	946066	59.80	0.30	12.72	2.62	0.15	0.30	7.39	0.22	7.38	0.89	6.80	99.69
HH_13	261538	946080	60.74	0.33	14.10	4.56	0.13	2.21	5.06	3.61	6.86	0.56	0.41	99.71
HH_19	261588	946087	54.71	0.58	14.52	5.26	0.14	2.47	6.29	2.93	6.82	1.08	2.48	99.02
HH_22	261580	946076	53.65	0.33	12.46	7.16	0.17	2.62	8.14	3.06	5.10	1.39	0.47	96.75
HH_25	261419	946629	52.90	0.75	9.25	7.55	0.30	4.93	13.47	2.49	4.36	1.87	0.1	99.38
HH_26	261314	946837	53.31	0.78	8.58	5.98	0.23	6.11	14.40	2.11	4.65	2.11	0.17	99.99
HH_30	260474	945199	58.50	0.63	13.73	5.12	0.19	1.89	6.28	3.70	6.88	0.76	0.16	99.03
HH_32	260861	945394	52.70	0.30	13.28	7.23	0.23	3.03	9.91	2.72	5.18	1.61	0.27	99.91
HH_34	260953	945524	48.80	2.65	3.82	15.05	0.56	5.25	17.98	2.03	1.69	1.17	−0.03	99.61
Cnoc nan Cuilean biotite–magnetite veins														
NWR-023	261566	946067	43.65	0.52	9.84	10.80	0.20	3.92	13.31	1.75	2.22	2.18	2.08	93.62
HH_15	261528	946079	50.41	0.50	10.46	8.34	0.25	3.39	11.39	2.83	4.55	2.99	0.68	97.26
HH_18	261558	946087	49.67	1.33	13.22	9.42	0.20	4.33	8.84	3.20	4.09	1.52	1.12	98.46

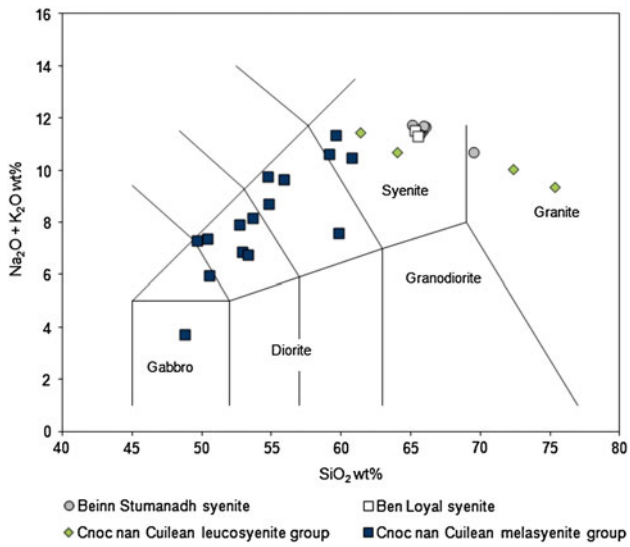

Fig. 9 Total alkali versus silica classification for all Loch Loyal Complex lithologies. Nomenclature is based on Middlemost (1994)

anomaly is likely to be a signature of subduction-related magmatism (Fowler et al. 2008), although it could also indicate crustal contamination. The Ti and P troughs may have been generated by early apatite and titanite fractionation.

The REE and Ba, Sr and Th are notably enriched in the melasyenite over the leucosyenite, and the highest contents are found in some biotite–magnetite vein samples. However, the overall trace element pattern in the biotite–magnetite veins is similar to that in the melasyenite, supporting the hypothesis that these veins formed by extensive hydrothermal alteration of melasyenite rather than by introduction of a later magmatic component.

Rare Earth Elements

Rare Earth Element data were normalised to chondrite using normalising factors from McDonough and Sun (1995), and REE plots are shown in Fig. 12. As with the trace elements, the REE plots for each lithology show very similar, smooth patterns with enrichment in the LREE, large La/Yb ratios (usually between 50 and 100), and no Eu anomalies. The patterns for the Ben Loyal and Beinn Stumanadh syenites are very similar to the Cnoc nan Cuilean leucosyenite. Total REE contents decrease with increasing SiO_2, and thus, the Cnoc nan Cuilean melasyenite has distinctly higher REE contents than the leucosyenite (Fig. 12a, b). This can be attributed to the REE exhibiting compatible behaviour at a relatively early stage of magma evolution, with crystallisation of REE-bearing accessory phases such as allanite, titanite and apatite in the melasyenite (Fowler et al. 2008). The parental magmas are likely to have been characterised by very high REE contents.

The biotite–magnetite veins have a similar REE pattern to the melasyenite, with significant enrichment in the LREE. Some samples show a distinct positive Ce anomaly (Fig. 11c), which may be due to the presence of oxidised Ce^{4+} in cerianite formed by alteration of other REE minerals (Styles and Young 1983).

Rare Earth Element data were converted to Total Rare Earth Oxide (TREO) for consistency with reported grades from deposits currently being evaluated for REE extraction. The highest REE values are present in the biotite–magnetite veins with TREO values of up to 20,000 ppm. As discussed, the melasyenite is more enriched than the leucosyenite with average values of 3,800 and 1,400 ppm REO, respectively. All lithologies are LREE dominated (as is the case with most REE deposits) with <3 % HREE. Ce represents nearly 50 % of the total REE content in the mela- and leucosyenite, whilst in the biotite–magnetite veins, it averages 68 % of the total REE content.

Discussion

The Cnoc nan Cuilean intrusion contains the highest TREO values known from any igneous rocks in the UK, and the new data presented here allow us to consider the processes by which the REE have been concentrated in this intrusion. Any model for REE enrichment must incorporate the following points:

1. The Loch Loyal Syenite Complex as a whole has high REE contents compared to rocks of similar composition elsewhere in the UK (Fowler et al. 2008), indicating that the original magmas were characterised by high REE contents.
2. The melasyenite has much higher REE contents than the leucosyenite, indicating early compatibility of the REE during crystallisation.
3. The highest REE contents occur in hydrothermally altered veins within the Mixed Zone syenite. The source of these hydrothermal fluids, and the processes by which the REE were concentrated, needs to be understood.

These issues are explored in more detail below.

Origin of the REE enrichment in the source magmas at Loch Loyal

The Loch Loyal Syenite Complex is part of a group of high Ba-Sr granite and syenite plutons with minor mafic to ultramafic and carbonatitic components, occurring throughout the Northern Highlands (Thompson and Fowler

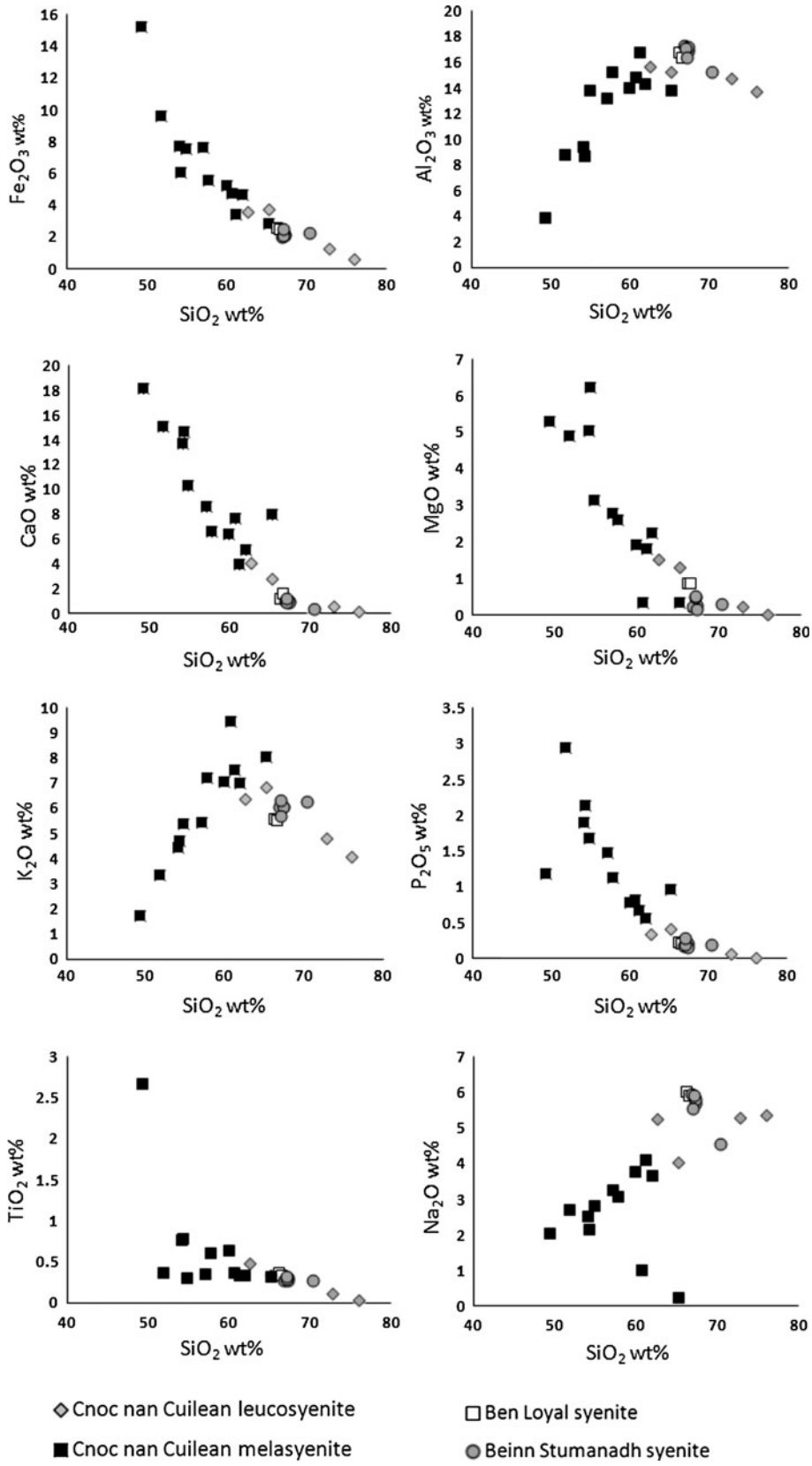

Fig. 10 Major element variations for all Loch Loyal Complex lithologies

Table 3 Trace and Rare Earth Element data for all Loch Loyal Syenite Complex lithologies

	Ba (ppm)	Rb (ppm)	Th (ppm)	Nb (ppm)	Ta (ppm)	Sr (ppm)	P (ppm)	Zr (ppm)	Hf (ppm)	Ti (ppm)	Tb (ppm)	Y (ppm)	La (ppm)
Ben Loyal syenite													
NWR-005	4,200	104	45	24.5	1.2	1,500	1,170	393	10.3	2,440	1.2	23.2	222
NWR-006	4,930	108	49	24.4	1.1	1,750	1,200	380	9.2	2,440	1.2	23.2	124
NWR-007	2,280	106	55	24.2	1.0	560	600	338	10.0	1,500	0.8	16.8	110
HH_4	4,000	96	47	23.7	1.1	1,100	1,290	401	9.1	2,450	1.5	28.7	234
Beinn Stumanadh syenite													
NWR-012	3,880	104	43	18.4	0.8	1,520	860	287	7.5	1,900	0.9	17.8	157
NWR-013	5,170	94	37	16.0	0.7	1,210	900	335	8.5	1,690	1.0	18.8	170
NWR-014	4,320	93	32	15.9	0.7	1,300	746	292	7.5	1,740	0.9	19.0	147
NWR-015	4,920	116	52	19.0	0.9	1,590	1,050	315	8.5	2,000	1.2	24.7	211
NWR-017	3,770	106	14	19.8	0.9	1,590	900	136	3.9	1,700	1.0	19.5	135
NWR-018	3,470	130	57	21.8	1.0	1,450	887	413	11.3	1,790	0.8	18.0	95
NWR-019	4,930	110	75	27.6	1.0	1,170	1,630	309	8.6	2,070	1.9	31.5	377
Cnoc nan Cuilean leucosyenite													
NWR-009	5,890	94	47	22.5	0.9	2,440	2,220	437	10.1	2,090	2.0	32.8	264
NWR-010	5,650	111	55	36.5	1.4	2,230	1,420	230	6.3	2,810	2.4	39.4	203
NWR-026	17,400	107	100	33.0	1.8	6,660	5,960	628	18.1	3,060	3.6	56.0	457
NWR-027	2,210	86	44	16.5	0.9	1,650	251	273	8.4	757	0.6	11.1	95
NWR-030	1,090	73	7	4.9	0.1	412	63	63	2.8	232	0.1	2.6	18
HH_8	4,850	75	31	23.7	1.2	2,040	1,420	421	9.2	3,000	2.1	37.5	171
HH_12	4,500	74	77	16.3	0.8	1,750	1,370	254	6.9	1,650	2.2	33.1	613
HH_40	7,120	97	59	14.2	0.4	2,530	1,890	148	3.9	751	2.2	35.9	210
Cnoc nan Cuilean melasyenite													
NWR-009A	5,790	42	318	18.4	0.8	2,960	13,200	408	11.3	2,250	13.5	175	1,120
NWR-020	10,900	99	127	37.5	1.8	5,450	2,900	584	17.3	2,170	2.7	40.4	528
NWR-021	10,300	152	264	46.0	2.7	2,290	3,550	401	11.7	2,320	6.6	93.9	534
NWR-022	5,740	165	268	25.2	1.1	1,810	4,320	268	7.5	2,060	5.7	72.7	1,300
NWR-024	12,000	99	56	17.1	1.0	4,190	2,370	238	7.1	1,520	2.1	32.5	149
NWR-025	5,025	83	80	66.9	2.1	1,760	3,220	244	7.6	5,940	5.2	91.3	382
NWR-028	6,905	107	97	45.8	3.0	3,220	4,230	633	19.6	3,630	4.0	65.3	364
HH_6	11,400	73	131	119	4.7	3,850	5,480	1,521	38.6	5,420	6.1	87.7	761
HH_9	9,670	115	76	31.1	1.9	3,005	10,900	711	18.8	5,550	4.2	57.2	253
HH_13	5,930	86	48	18.2	0.8	2,700	2,440	641	13.9	1,990	2.4	40.2	288
HH_15	4,970	64	547	28.2	1.4	2,650	13,200	395	9.4	2,750	12.2	147	1,700
HH_20	10,800	120	184	37.1	2.0	3,390	4,650	732	19.1	3,000	5.3	62.3	1,270
HH_25	7,700	62	165	74.6	3.5	2,520	8,020	384	10.6	4,300	8.7	122	444

Table 3 continued

	Ba (ppm)	Rb (ppm)	Th (ppm)	Nb (ppm)	Ta (ppm)	Sr (ppm)	P (ppm)	Zr (ppm)	Hf (ppm)	Ti (ppm)	Tb (ppm)	Y (ppm)	La (ppm)
HH_26	8,590	78	62	59.5	0.9	2,760	9,410	289	7.6	4,950	5.7	87.2	437
HH_30	7,470	95	58	42.3	1.7	1,700	2,850	224	6.1	3,590	4.7	68.3	264
HH_32	24,800	80	90	6.7	0.3	5,870	7,610	415	10.1	1,890	4.9	68.4	476
HH_34	1,690	31	161	177	6.4	1,260	5,820	516	14.5	17,200	12.2	185	810
HH_35	10,100	117	180	36.4	1.8	3,260	4,130	557	12.9	2,550	6.7	98.6	645
Cnoc nan Cuilean pegmatite													
NWR-011	4,970	106	85	30.6	1.1	1,720	3,410	111	3.8	2,250	4.2	62.2	397
NWR-029	4,690	91	464	56.7	2.4	2,300	14,800	454	13.3	2,370	13.0	192	1,280
Cnoc nan Cuilean bt-mag veins													
NWR-023	1,780	37	28	28.7	1.3	3,340	11,500	381	11.2	3,790	10.7	68.6	937
HH_14	3,120	44	904	15.7	0.8	2,140	19,500	251	6.3	3,300	13.3	154	954
HH_18	4,990	59	389	71.4	3.5	2,860	7,000	424	10.1	8,080	8.2	95.0	2,470
HH_21	2,050	24	4	6.8	0.7	2,290	2,150	382	9.3	2,610	9.2	48.3	1,680

	Ce (ppm)	Pr (ppm)	Nd (ppm)	Sm (ppm)	Eu (ppm)	Gd (ppm)	Tb (ppm)	Dy (ppm)	Ho (ppm)	Er (ppm)	Tm (ppm)	Yb (ppm)	Lu (ppm)
Ben Loyal syenite													
NWR-005	343	41	143	20	4.5	10.7	1.2	5.4	0.8	2.0	0.3	1.6	0.2
NWR-006	308	33	123	19	4.6	10.5	1.2	5.5	0.8	2.0	0.2	1.5	0.2
NWR-007	207	22	81	12	2.8	6.5	0.8	3.4	0.5	1.4	0.2	1.1	0.2
HH_4	430	49	172	25	5.7	13.5	1.5	6.5	1.0	2.4	0.3	1.8	0.2
Beinn Stumanadh syenite													
NWR-012	300	31	109	15	3.6	8.1	0.9	4.0	0.6	1.4	0.2	1.1	0.2
NWR-013	323	34	120	16	3.9	8.7	1.0	4.3	0.6	1.5	0.2	1.2	0.2
NWR-014	281	30	106	15	3.6	8.2	0.9	4.2	0.6	1.5	0.2	1.0	0.2
NWR-015	379	42	146	21	4.7	10.7	1.2	5.3	0.7	1.9	0.2	1.3	0.2
NWR-017	276	32	117	17	4.1	8.9	1.0	4.4	0.7	1.5	0.2	1.1	0.2
NWR-018	229	20	74	11	2.7	6.2	0.8	3.6	0.6	1.5	0.2	1.3	0.2
NWR-019	804	90	318	41	8.9	18.9	1.9	7.7	1.1	2.4	0.3	1.7	0.2
Cnoc nan Cuilean leucosyenite													
NWR-009	566	64	241	35	8.0	18.9	2.0	8.5	1.2	2.9	0.3	2.1	0.3
NWR-010	576	68	263	40	9.0	21.0	2.4	10.1	1.4	3.2	0.4	2.2	0.3
NWR-026	978	110	415	62	14.3	33.2	3.6	14.6	2.0	4.4	0.5	2.7	0.4
NWR-027	233	21	71	10	2.3	5.0	0.6	2.5	0.4	0.8	0.1	0.7	0.1
NWR-030	41	4	14	2	0.5	1.1	0.1	0.6	0.1	0.2	0.0	0.2	0.0
HH_8	472	57	216	34	7.9	18.9	2.1	9.1	1.3	3.1	0.4	2.2	0.3
HH_12	993	117	397	48	9.4	22.3	2.2	8.7	1.2	2.7	0.3	1.8	0.3

Table 3 continued

	Ce (ppm)	Pr (ppm)	Nd (ppm)	Sm (ppm)	Eu (ppm)	Gd (ppm)	Tb (ppm)	Dy (ppm)	Ho (ppm)	Er (ppm)	Tm (ppm)	Yb (ppm)	Lu (ppm)
HH_40	486	61	238	37	8.3	20.9	2.2	9.3	1.3	2.9	0.3	1.9	0.3
Cnoc nan Cuilean melasyenite													
NWR-009A	2,490	304	1,250	219	47.5	127	13.5	54.1	7.2	15.0	1.6	8.7	1.2
NWR-020	1,050	106	371	52	11.6	25.1	2.7	10.8	1.4	3.1	0.4	2.0	0.3
NWR-021	1,430	184	744	119	25.8	62.8	6.6	26.6	3.5	7.3	0.8	4.2	0.6
NWR-022	2,500	278	1,010	131	25.4	57.9	5.7	21.3	2.7	5.5	0.6	3.3	0.5
NWR-024	367	47	199	35	8.4	19.3	2.1	8.9	1.2	2.6	0.3	1.7	0.3
NWR-025	974	132	534	88	20.0	47.5	5.2	22.7	3.2	7.3	0.9	5.3	0.8
NWR-028	955	111	429	68	15.0	36.3	4.0	16.5	2.2	4.9	0.6	3.2	0.4
HH_6	1,650	180	677	106	23.2	57.1	6.1	25.4	3.5	7.7	0.8	4.7	0.6
HH_9	689	91	387	68	15.3	39.2	4.2	16.9	2.2	4.7	0.5	2.7	0.4
HH_13	604	71	264	39	9.0	22.6	2.4	10.1	1.4	3.3	0.4	2.4	0.4
HH_15	3,840	434	1,500	228	45.3	120	12.2	46.6	6.1	12.7	1.4	7.1	1.0
HH_20	2,180	245	853	112	22.5	53.2	5.3	19.1	2.5	5.1	0.6	3.1	0.4
HH_25	1,400	196	833	148	32.0	84.2	8.7	36.4	4.9	10.7	1.2	6.4	0.9
HH_26	1,160	152	606	97	21.6	54.0	5.7	24.0	3.3	7.4	0.8	4.8	0.6
HH_30	846	108	454	77	17.3	44.0	4.7	19.7	2.7	5.9	0.7	3.9	0.5
HH_32	1,050	123	490	81	18.4	46.9	4.9	20.1	2.7	5.9	0.7	3.9	0.6
HH_34	2,270	311	1,270	211	46.2	117	12.2	53.5	7.5	17.0	2.0	12.0	1.8
HH_35	1,710	208	805	122	26.2	66.0	6.7	28.0	3.8	8.6	0.9	4.9	0.6
Cnoc nan Cuilean pegmatite													
NWR-011	1,070	123	484	75	16.0	39.6	4.2	17.0	2.3	5.2	0.6	3.5	0.5
NWR-029	3,150	397	1,540	236	49.9	123	13.0	51.8	7.0	15.1	1.7	8.6	1.1
Cnoc nan Cuilean bt-mag veins													
NWR-023	14,000	299	1,510	200	41.7	109	10.7	40.9	5.0	10.1	1.1	5.4	0.8
HH_14	2,580	320	1,150	202	42.4	118	13.3	48.2	6.4	12.9	1.4	6.9	0.9
HH_18	4,510	473	1,480	178	33.8	81.0	8.2	29.6	3.9	8.2	0.9	4.7	0.6
HH_21	8,160	503	2,000	223	42.0	101	9.2	31.4	3.8	7.1	0.8	4.4	0.7

1986; Fowler et al. 2001, 2008). These plutons all have characteristic trace element patterns, including enrichment in Ba, Sr and the LREE, but relatively low contents of high field strength elements such as Nb, Ta and Th (Tarney and Jones 1994; Fowler et al. 2008). The ultimate source of these magmas is now generally thought to be in mantle that was modified by the subduction of Iapetus ocean crust below Laurentia (Fowler et al. 2008).

Fowler et al. (2008) used samples from the Ben Loyal intrusion to show that the Loch Loyal Syenite Complex had similar REE patterns, but notably high LREE contents, when compared with all other plutons in the Northern Highlands high Ba-Sr suite. Whereas the Ben Loyal intrusion is composed of relatively homogeneous leucosyenite, Cnoc nan Cuilean contains abundant more mafic lithologies with yet higher REE contents, and Cnoc nan Cuilean is thus the most REE-enriched intrusion in the Northern Highlands by a significant margin. There are no isotopic data for the Cnoc nan Cuilean lithologies, but as there is a good inverse correlation between contents of the LREE and SiO_2 for all rock-types from the Loch Loyal Syenite Complex, it is likely that they were all derived from the same magmatic source which subsequently underwent fractional crystallisation. The presence of the highest REE contents in the most mafic lithologies demonstrates that this enrichment must have been present in the mantle-derived parental magmas and cannot be attributed to subsequent assimilation of local crustal material. Saturation levels for the LREE in felsic magmas are relatively low, but are significantly higher in mafic magmas (Miller and Mittlefehldt 1982); the early onset of allanite crystallisation at Cnoc nan Cuilean thus indicates high LREE contents in the parental magmas. Similar inverse correlations between REE and SiO_2 content have been recorded in another suite of mixed magmas within the Northern Highlands suite, the Ach'Uaine hybrids (Fowler and Henney 1996), although these do not attain REE concentrations as high as those observed at Cnoc nan Cuilean.

On the basis of isotopic and trace element evidence, Fowler et al. (2008) have proposed that the parental magmas to the high Ba–Sr intrusions were derived from a Caledonian Parental Magma Array (CPMA) that extended from isotopically and elementally depleted to enriched compositions. Loch Loyal was shown to lie at the enriched end of this array, with ε_{Nd} values around −6. The sources of these magmas are considered to have been in subduction-modified lithospheric mantle, with the introduction of a carbonate component explaining the high Ba–Sr signatures. Two possibilities have been proposed for this carbonate component: earlier carbonatite-derived metasomatism of the lithospheric mantle during extension (Goodenough et al. 2004), or introduction of pelagic sediments, which are typically enriched in Ba, Sr and the LREE (Plank and Langmuir 1998), during subduction. Introduction of around 10 % of such sediment can be modelled to fit the isotopically enriched end of the CPMA (Fowler et al. 2008) and thus provides the best available fit for existing data.

Similar features have been recognised in the Cenozoic Mianning-Dechang REE belt in the Sichuan province of China (Hou et al. 2009). This belt of syenite–carbonatite igneous complexes, intruded into a Cenozoic collisional zone, is associated with several REE deposits including the giant Maoniuping deposit (Hou et al. 2006, 2009; Xu et al. 2008). The syenite and associated carbonatite intrusions in this area have high Ba, Sr and LREE contents, but are low in the HFSE and are isotopically enriched (low ε_{Nd}, high $^{87}Sr/^{86}Sr$). They thus provide an excellent analogue for the Loch Loyal Syenite Complex and other enriched members of the CPMA. A component of subducted carbonate-rich pelagic sediment has been proposed as the source of the chemical characteristics of these Chinese magmas and hence also of the major REE deposits (Hou et al. 2006). This igneous belt is thus a good analogue for the Northern Highlands igneous suite.

Concentration of the REE in more mafic lithologies

Within the Loch Loyal Syenite Complex, and especially in Cnoc nan Cuilean where substantial compositional variation is recognised, the REE are clearly more abundant in the more mafic lithologies. This pattern is unusual, because the REE are generally considered to behave incompatibly and thus should be enriched in the more evolved, silicic lithologies, although crystallisation of allanite is known to remove the LREE from the most evolved magmas in some cases (Miller and Mittlefehldt 1982). Similar features have been recorded in some other suites (Sawka et al. 1984). Such patterns are also recognised in other intrusions of the Northern Highlands suite, notably in the Ach'Uaine Hybrid appinites which also include a wide range of compositions (Fowler and Henney 1996).

The inverse correlation of the REE with SiO_2 can be attributed to fractional crystallisation of a mantle-derived basic magma that was close to saturation in the LREE, leading to early development of REE-rich accessory minerals such as apatite, titanite and allanite (Fowler et al. 2008). At Cnoc nan Cuilean, crystallisation of the REE-enriched parental magma led to the formation of early euhedral mineral phases such as clinopyroxene, titanite and apatite. This was followed by the later crystallisation of other magmatic phases, chiefly feldspars, with late-magmatic allanite forming as rims round apatite and interstitial to earlier minerals. Much of the REE budget of the magma was taken up by the allanite, apatite and titanite at this early stage of magmatic evolution, so that the more evolved leucosyenite has lower REE contents.

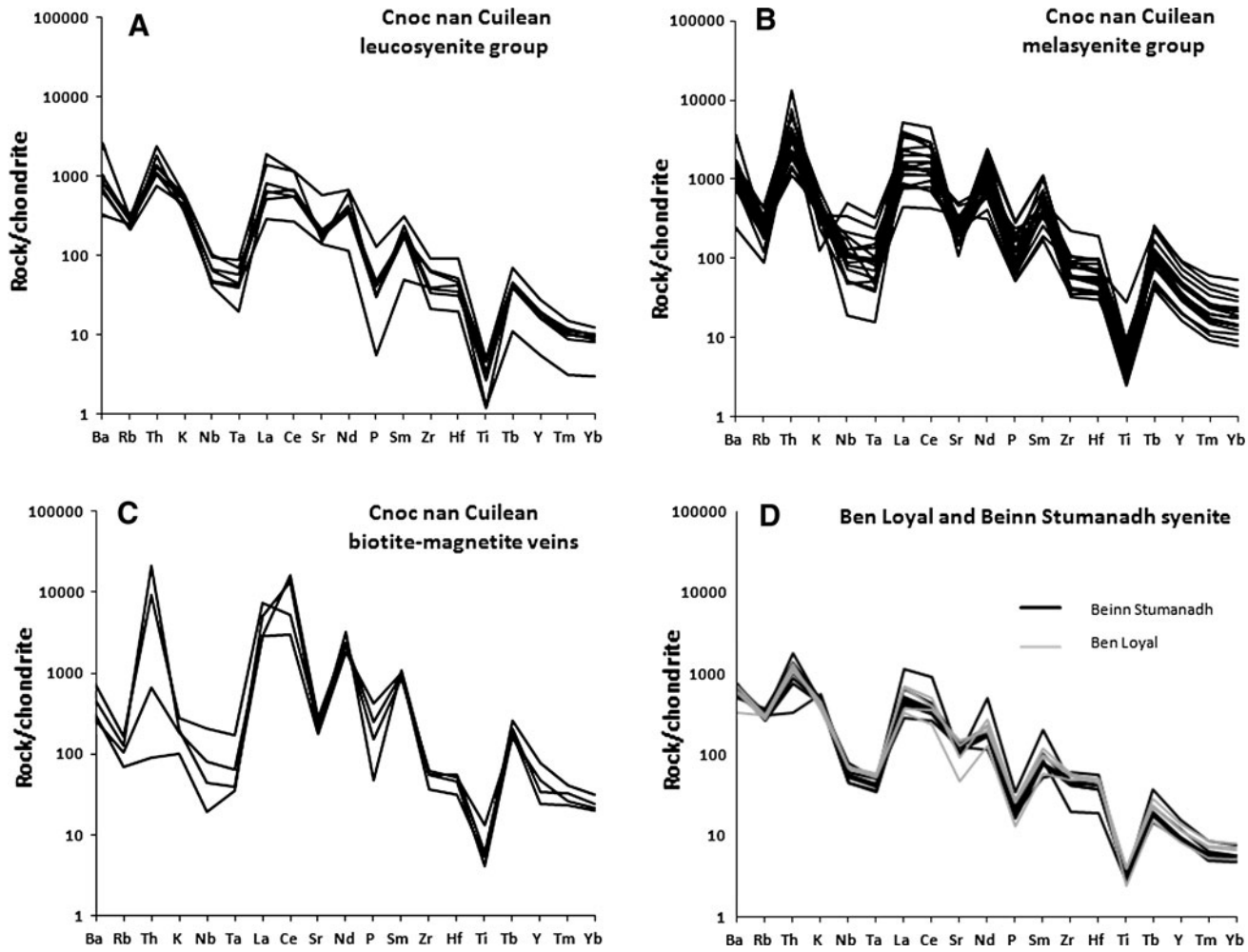

Fig. 11 Multi-element chondrite-normalised plots for all Loch Loyal Complex lithologies. Normalising factors from McDonough and Sun (1995)

Mobilisation and enrichment of REE

As described above, the REE are most significantly enriched in the more mafic melasyenite of Cnoc nan Cuilean, where they are hosted in late-magmatic allanite. The melasyenite was partially crystallised by the time that a leucosyenitic magma was introduced into the magma chamber, creating the Mixed Syenite Zone with examples of magma mixing and mingling, and the overlying Massive Leucosyenite Zone. Cooling and crystallisation within this magma chamber led to fracturing of the syenite, and these fractures were then infilled by allanite micro-veinlets. Such micro-veinlets are present throughout the syenite intrusion, and formation of these is attributed to a late-magmatic–hydrothermal system.

Subsequently, an episode of microgranite veining crosscuts and offsets these allanite micro-veinlets. At approximately the same time, alteration of the syenite in the Mixed Syenite Zone by hydrothermal fluids circulating along cracks led to the development of discrete biotite–magnetite veins. The microgranite veins transect, and anastomose through, these biotite–magnetite veins. The early stages of formation of the biotite–magnetite veins appear to have been associated with the growth of large, often zoned crystals of allanite, magnetite, and apatite, and the alteration of many magmatic minerals to biotite. These fluids are likely to have been associated with very evolved magmas rising from depth in the magma chamber, which are now represented by the thin microgranite veins that represent the last magmatic event in the intrusion. The apatites that formed at this time are fluorapatites, indicating the likelihood that the fluids were also enriched in F. Complexing with fluoride is one of the main ways in which the LREE can be transported in hydrothermal fluids (Salvi and Williams-Jones 1990). The biotite–magnetite veins have only been recognised within the Mixed Syenite Zone, which already contained REE-enriched melasyenite, and this indicates that REE mobility occurred over relatively small spatial scales.

Subsequent events within the intrusion, and possibly introduction of a new batch of fluids, caused fracturing of

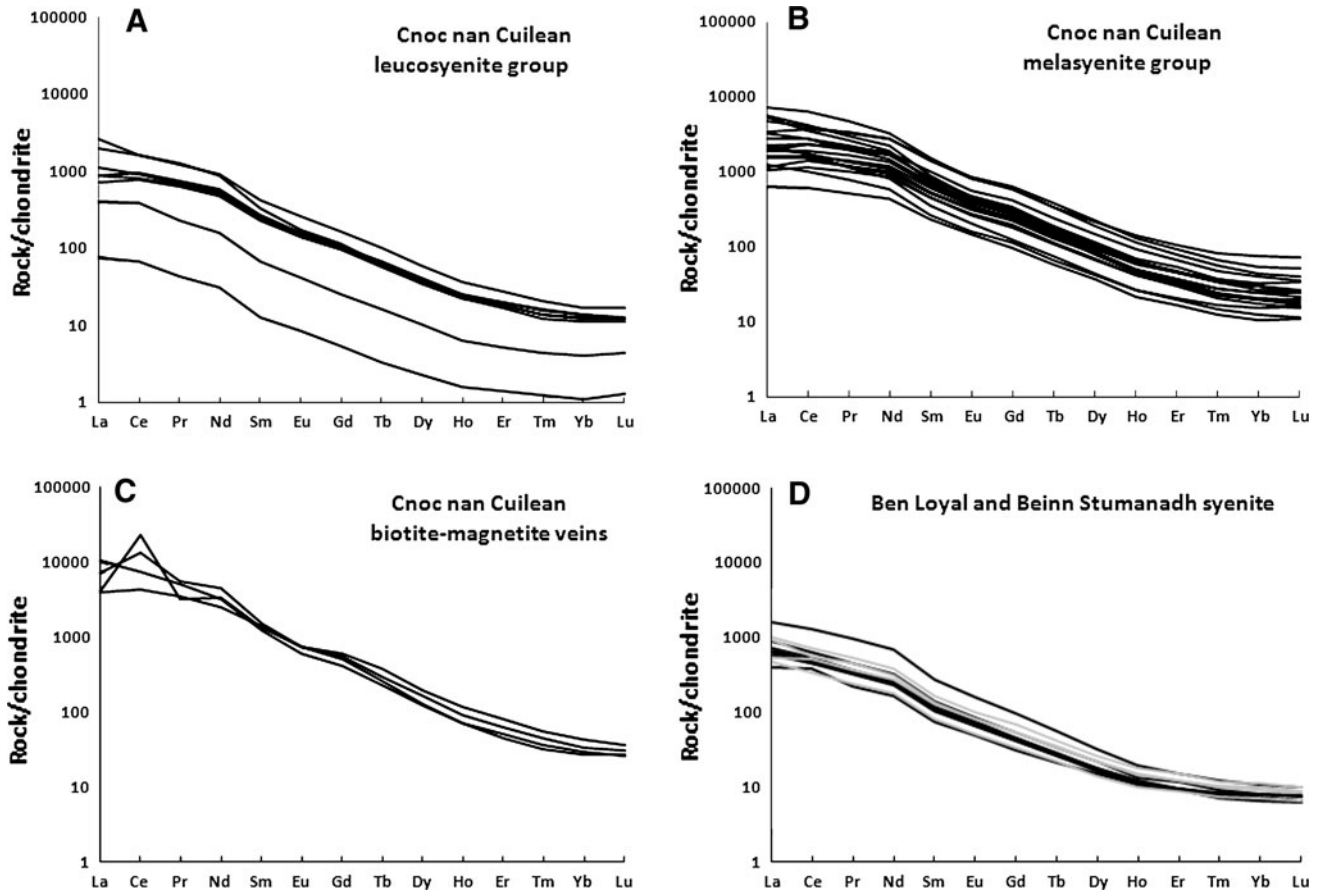

Fig. 12 Chondrite-normalised REE plots for all Loch Loyal Complex lithologies. Normalising factors from McDonough and Sun (1995)

the biotite–magnetite veins and alteration of the vein allanite. Alteration occurred preferentially along growth zoning. The altered, darker areas of the allanite show lower Al, Si, Ca and total REE contents but are relatively enriched in Sr, Th, Mn, Ti, F, P and Cl. The high Th contents may be derived from original growth zoning and may indicate that alteration was focused along zones that had been affected by metamictisation. Some altered, bright-coloured zones within allanite crystals are enriched in the REE, and results from U–Pb geochronology indicate the likelihood of open-system behaviour in these zones, with introduction of REE from outside the host crystal. REE leached from altered allanite were also incorporated into the fluid and reprecipitated into fractures, forming REE-Sr-carbonate and REE-carbonate veins. Although these contain greater concentrations of REE, their REE patterns are similar to the allanite. The presence of carbonate minerals suggests the possibility that these last fluids to circulate within the intrusion were carbonate rich.

Similar hydrothermal alteration is recorded in a number of other intrusions, notably the Thor Lake Syenite in Canada which hosts the Nechalacho Zr–Nb–REE deposit. Here, hydrothermal alteration of syenite has produced zones rich in magnetite and biotite which were temporally associated with the formation of a range of accessory minerals including allanite (Sheard et al. 2012). As at Cnoc nan Cuilean, these minerals both replaced earlier phases and infilled fractures in primary minerals. In the Shuiquangou syenitic complex, Northern China, hydrothermally altered syenite also exhibits the introduction of biotite and allanite (Jiang et al. 2003).

The hydrothermal fluids that concentrated the REE at Cnoc nan Cuilean were most probably derived from within the associated magma chamber, with mobility of REE on a scale no larger than that of the intrusion. However, it is also possible that they were introduced by exotic mineralising fluids. Both possibilities have been recognised in other localities enriched in the REE. Hydrothermal magnetite-apatite systems with REE enrichment, hosted in granitoid intrusions, have been investigated using Nd isotopes, and this work has shown that the REE are largely derived from their associated igneous rocks (Gleason et al. 2000). However, in other REE-mineralised deposits such as the Ivigtut pluton in Greenland and Olympic Dam in Australia, Nd isotope data have been used to show that exotic, mantle-derived fluids have introduced the REE and other

elements into hydrothermally altered granitoids (Johnson and McCulloch 1995; Goodenough et al. 2000). In the Shuiquangou complex, both late-magmatic and externally derived fluids have been inferred (Jiang et al. 2003).

Minerals from the Cnoc nan Cuilean biotite–magnetite veins contain very few fluid inclusions that would be suitable for study, and so fluid compositions can only be inferred from compositions of minerals in these veins. All the Cnoc nan Cuilean allanite has relatively similar compositions and REE patterns, and the late REE-carbonate minerals also have similar REE patterns. The chemical compositions of the REE minerals thus do not provide evidence for introduction of exotic fluids. However, the apparent introduction of carbonate ions into the intrusion at a late stage in its development, forming the REE-carbonate minerals in fractures, may indicate a relatively small component of late-stage exotic, carbonate-bearing fluid. Detailed isotope work would be required to elucidate the origins of these fluids.

At Cnoc nan Cuilean, detailed petrography and analysis of mineral chemistry have demonstrated the probability of three separate episodes of fluid circulation and hydrothermal alteration:

1. The first episode was related to crystallisation of the leucosyenite, with late-magmatic fluids circulating and depositing micro-veinlets of allanite into fractures throughout the syenite.
2. The second hydrothermal episode was focused in the Mixed Syenite Zone and formed the biotite–magnetite veins. This episode is considered to be related to the introduction of highly evolved, K-rich fluids related to small amounts of the final, highly evolved granitic magmas within the syenitic magma chamber. These fluids were enriched in F, allowing complexing and mobility of the REE and leading to the formation of fluorapatite and zoned allanite.
3. A subsequent, final hydrothermal event caused alteration of the zoned allanite and precipitation of Sr-enriched REE-carbonate minerals as thin veinlets. These late, carbonate-bearing fluids may have been derived from a source outwith the Cnoc nan Cuilean magma chamber. Minor carbonatites are known in the Northern Highlands igneous suite (Young et al. 1994), and it is possible that these latest fluids may be related to carbonatite activity at depth.

U–Pb geochronology gives imprecise ages for allanite and titanite in the biotite–magnetite veins, probably due to open-system behaviour and alteration. These ages overlap with the crystallisation age of zircon in the Cnoc nan Cuilean leucosyenite (Halliday et al. 1987) and do not allow distinction of the timing of the different hydrothermal events.

Conclusions

The Cnoc nan Cuilean intrusion of the Loch Loyal Syenite Complex is significantly enriched in the REE, with maximum TREO values up to 2 %, comparable with deposits currently being considered for exploitation. However, the full scale of this mineralisation is unknown, due to poor exposure of the friable veins in which the highest REE contents are found. Petrographic, geochemical and mineral chemistry data suggest that this REE enrichment is due to a combination of magmatic and post-magmatic processes.

The magmas from which the Loch Loyal Syenite Complex formed were markedly enriched in the REE, and the setting is analogous with similar intrusive suites in the Sichuan Province of China that host major REE deposits. On the basis of current data, the REE enrichment of the Northern Highlands magmas can be ascribed to the introduction of LREE-enriched pelagic carbonates into a Caledonian subduction zone (Fowler et al. 2008). Fluids derived from these carbonates and from the subducting slab were introduced into the mantle wedge, which then melted to produce REE-enriched parental magmas.

These parental magmas were saturated in the LREE, and as a consequence the LREE behaved compatibly. As the magmas began to crystallise in a crustal magma chamber at Cnoc nan Cuilean, LREE-rich minerals such as apatite and allanite were part of the mineral assemblage developed in early, relatively mafic melasyenite. These were subsequently intruded by leucosyenitic magmas that have lower REE contents. As the magma chamber cooled, circulating late-magmatic fluids deposited micro-veinlets of allanite.

The last magmatic episode in the Cnoc nan Cuilean magma chamber involved the emplacement of microgranitic veins, associated with highly evolved fluids that were K- and F-rich. These fluids caused pervasive hydrothermal alteration along discrete fluid pathways in the melasyenite, generating biotite–magnetite veins with abundant allanite and apatite, and high REE contents. The REE complexed with F in the fluids and were remobilised, then reprecipitated in the biotite–magnetite veins. A final episode of hydrothermal fluid activity followed the fluid pathways represented by these veins, and caused alteration of existing allanite with the precipitation of REE carbonate minerals. These fluids may have been derived from outside the Cnoc nan Cuilean magma chamber.

The extent of the REE-enriched biotite–magnetite veins at Cnoc nan Cuilean is not known, but by analogy with similar intrusions, it is likely that they have a significantly greater extent than can be recognised with the current exposure levels. Zones of hydrothermal alteration that are enriched in the LREE may also exist at depth beneath the other intrusions of the Loch Loyal Syenite Complex.

Acknowledgments Mike Fowler is thanked for productive discussions in the field. Paul Lusty is thanked for constructive comments on an earlier version of this paper. Chris McFarlane and an anonymous reviewer are thanked for review comments, which have significantly improved the paper. Editorial handling and insight by Franck Poitrasson are much appreciated. The authors publish with the permission of the Executive Director of the British Geological Survey.

References

ASTM-Standard-E1508 (2012a) Designation: E1508-12a. Standard guide for quantitative analysis by energy-dispersive spectroscopy. ASTM-International, West Conshohocken, PA. doi: 10.1520/E1508-12A

Chakhmouradian AR, Wall F (2012) Rare earth elements: minerals, mines, magnets (and more). Elements 8:333–346

Chakhmouradian AR, Zaitsev AN (2012) Rare earth mineralization in igneous rocks: sources and processes. Elements 8:347–353

Deer WA, Howie RA, Zussman J (1992) An introduction to the rock-forming minerals. Longman Scientific & Technical, Harlow

Drake MJ, Weill DF (1972) New rare earth standards for electron microprobe analysis. Chem Geol 10:179–181

Fowler MB, Henney PJ (1996) Mixed Caledonian appinite magmas: implications for lamprophyre fractionation and high Ba–Sr granite genesis. Contrib Mineral Petrol 126:199–215

Fowler MB, Henney PJ, Darbyshire DPF, Greenwood PB (2001) Petrogenesis of high Ba–Sr granites: the Rogart pluton, Sutherland. J Geol Soc Lond 158:521–534

Fowler MB, Kocks H, Darbyshire DPF, Dreenwood PB (2008) Petrogenesis of high Ba–Sr plutons from the northern highlands Terrane of the British Caledonian Province. Lithos 105:129–148

Ghent ED (1972) Electron microprobe study of allanite from the Mt. Falconer quartz monzonite pluton, Lower Taylor Valley, South Victoria Land, Antarctica. Can Mineral 11:526–530

Gleason JD, Marikos MA, Barton MD, Johnson DA (2000) Neodymium isotopic study of rare earth element sources and mobility in hydrothermal Fe oxide (Fe-P-REE) systems. Geochim Cosomochim Acta 64:1059–1068

Goodenough KM, Upton BGJ, Ellam RM (2000) Geochemical evolution of the Ivigtut granite, South Greenland: a fluorine-rich ''A-type'' intrusion. Lithos 51:205–221

Goodenough KM, Young BN, Parsons I (2004) The minor intrusions of Assynt, NW Scotland: early development of magmatism along the Caledonian Front. Mineral Mag 68:541–559

Goodenough KM, Millar I, Strachan RA, Krabbendam M, Evans JA (2011) Timing of regional deformation and development of the Moine Thrust Zone in the Scottish Caledonides: constraints from the U–Pb geochronology of alkaline intrusions. J Geol Soc Lond 168:99–114

Gregory CJ, Rubatto D, Allen CM, Williams IS, Hermann J, Ireland T (2007) Allanite microgeochronology: a LA-ICP-MS and SHRIMP U–Th–Pb study. Chem Geol 245:162–182

Halliday AN, Aftalion M, Parsons I, Dickin AP, Johnson MRW (1987) Syn-orogenic alkaline magmatism and its relationship to the Moine Thrust Zone and the thermal state of the Lithosphere in NW Scotland. J Geol Soc Lond 144:611–617

Hatch GP (2012) Dynamics in the global market for rare earths. Elements 8:341–346

Holdsworth RE, McErlean MA, Strachan RA (1999) The influence of country rock structural architecture during pluton emplacement: the Loch Loyal syenites, Scotland. J Geol Soc Lond 156:163–175

Holdsworth RE, Strachan RA, Alsop GI (2001) Solid geology of the Tongue District: memoir for 1:50,000 Geological Sheet 114E (Scotland). British Geological Survey, Keyworth

Hou Z, Tian S, Yuan Z, Xie Y, Yin S, Yi L, Fei H, Yang Z (2006) The Himalayan collision zone carbonatites in western Sichuan, SW China: petrogenesis, mantle source and tectonic implication. Earth Planet Sci Lett 244:234–250

Hou Z, Tian S, Xie Y, Yang Z, Yuan Z, Yin S, Yi L, Fei H, Zou T, Bai G, Li X (2009) The Himalayan Mianning–Dechang REE belt associated with carbonatite–alkaline complexes, eastern Indo-Asian collision zone, SW China. Ore Geol Rev 36:65–89

Hughes HSR, Goodenough KM, Walters AS, McCormac M, Gunn AG, Lacinska A (2013) The structure and petrology of the Cnoc nan Cuilean Intrusion, Loch Loyal Syenite Complex, north-west Scotland. Geol Mag. http://dx.doi.org/10.1017/S0016756812000957

Jiang N, Sun S, Chu X, Mizuta T, Ishiyama D (2003) Mobilization and enrichment of high-field strength elements during late- and post-magmatic processes in the Shuiquangou syenitic complex, Northern China. Chem Geol 200:117–128

Jochum KP, Weis U, Stoll B, Kuzmin D, Yang Q, Raczek I, Jacob DE, Stracke A, Birbaum K, Frick DA, Gunther D, Enzweiler J (2011) Determination of reference values for NIST SRM 610–617 glasses following ISO guidelines. Geostand Geoanal Res 35:397–429

Johnson JP, McCulloch MT (1995) Sources of mineralising fluids for the Olympic Dam deposit (South Australia): Sm–Nd isotopic constraints. Chem Geol 121:177–199

King BC (1942) The Cnoc nan Cuilean area of the Ben Loyal Igneous Complex. Q J Geol Soc 98:147–185

McDonough WF, Sun SS (1995) The composition of the Earth. Chem Geol 120:223–253

Middlemost EAK (1994) Naming materials in the magma/igneous rock system. Earth-Sci Rev 37:215–224

Miller CF, Mittlefehldt DW (1982) Depletion of light rare-earth elements in felsic magmas. Geology 10:129–133

Morin JA (1977) Allanite in granitic rocks of the Kenora-Vermilion Bay area, Northwestern Ontario. Can Mineral 15:297–302

Palin RM, Searle MP, Waters DJ, Horstwood MSA, Parrish RR, Roberts NMW, Yeh M-W, Chung S-L, Anh TT (2013) A geochronological and petrological study of anatectic paragneiss and associated granite dykes from the Day Nui Con Voi metamorphic core complex, North Vietnam; constraints upon the timing of metamorphism within the Red River shear zone. J Metamorph Geol 31:359–387

Parsons I (1972) Comparative petrology of the leucocratic syenites of the Northwest Highlands of Scotland. Geol J 8:71–82

Parsons I (1999) Late Ordovician to mid-Silurian alkaline intrusions of the North-west Highlands of Scotland. In: Stephenson D, Bevins RE, Milward D, Highton AJ, Parsons I, Stone P, Wadsworth WJ (eds) Caledonian igneous rocks of Great Britain geological conservation review, vol 17. Joint Nature Conservation Committee, Peterborough, pp 345–393

Petrik I, Broska I, Lipka J, Siman P (1995) Granitoid allanite–(Ce); substitution relations, redox conditions and REE distributions (on an example of I-type granitoids, Western Carpathians, Slovakia). Geol Carpathica 46:79–94

Plank T, Langmuir CH (1998) The chemical composition of subducting sediment and its consequences for the crust and mantle. Chem Geol 145:325–394

Poitrasson F (2002) In situ investigations of allanite hydrothermal alteration: examples from calc-alkaline and anorogenic granites

of Corsica (southeast France). Contrib Mineral Petrol 142:485–500

Pouchou JL, Pichoir F, Bovin D (1990) The XPP procedure applied to quantitative EDS X-ray analysis in the SEM. In: Michael JR, Ingram P (eds) Microbeam analysis. San Francisco Press, San Francisco, pp 120–126

Roberts NMW, Smye AJ, Condon DJ, Horstwood MSA (2012) Ancient allanite; time-teller or time-waster? In: Metamorphic Studies Group Research in progress meeting, Cambridge

Robertson RCR, Parsons I (1974) The Loch Loyal syenites. Scott J Geol 10:129–146

Salvi S, Williams-Jones AE (1990) The role of hydrothermal processes in the granite-hosted Zr, Y, REE deposit at Strange Lake, Quebec/Labrador: evidence from fluid inclusions. Geochim Cosomochim Acta 54:2403–2418

Salvi S, Williams-Jones AE (2005) Alkaline granite-syenite deposits. In: Linnen RL, Samson IM (eds) Rare-element geochemistry and mineral deposits. Geological Association of Canada Short Course Notes 17, pp 315–341

Sawka WN, Chappell BW, Norrish K (1984) Light-rare-earth-element zoning in sphene and allanite during granitoid fractionation. Geology 12:131–134

Schmitz MD, Bowring SA (2001) U–Pb zircon and titanite systematics of the Fish Canyon Tuff: an assessment of high-precision U–Pb geochronology and its application to young volcanic rocks. Geochim Cosomochim Acta 65:2571–2587

Shaw MH, Gunn AG (1993) Rare earth elements in alkaline intrusions, North-West Scotland. Mineral Reconnaissance Programme, Open File Report 11. Keyworth, Nottingham

Sheard ER, Williams-Jones AE, Heiligmann M, Pederson C, Trueman DL (2012) Controls on the concentration of zirconium, niobium, and the rare earth elements in the Thor Lake rare metal deposit, Northwest Territories, Canada. Econ Geol 107:81–104

Spencer KJ, Hacker BR, Kylander-Clark ARC, Andersen TB, Cottle JM, Stearns MA, Poletti JE, Seward GGE (2013) Campaign-style titanite U–Pb dating by laser ablation ICP: implications for crustal flow, phase transformations and titanite closure. Chem Geol 341:84–101

Stacey JS, Kramers JD (1975) Approximation of terrestrial lead isotope evolution by a two-stage model. Earth Planet Sci Lett 26:207–221

Styles MT, Young BR (1983) Fluocerite and its alteration products from the Afu Hills, Nigeria. Mineral Mag 47:41–46

Tarney J, Jones CE (1994) Trace element geochemistry of orogenic igneous rocks and crustal growth models. J Geol Soc Lond 151:855–868

Thomas RJ, Roberts NMW, Jacobs J, Bushid AM, Horstwood MSA, Mruma A (2013) Structural and geochronological constraints on the evolution of the eastern margin of the Tanzania Craton in the Mpwapwa area, central Tanzania. Precambr Res 224:671–689

Thompson RN, Fowler MB (1986) Subduction-related shoshonitic and ultrapotassic magmatism: a study of Siluro-Ordovician syenites from the Scottish Caledonides. Contrib Mineral Petrol 94:507–522

Vlach RFS, Gualda GAR (2007) Allanite and chevkinite in A-type granites and syenites of the Graciosa Province, southern Brazil. Lithos 97:98–121

Wood SA, Ricketts A (2000) Allanite-(Ce) from the Eocene Casto Granite, Idaho: response to hydrothermal alteration. Can Mineral 38:81–100

Xu C, Campbell IH, Kynicky J, Allen CM, Chen Y, Huang Z, Qi L (2008) Comparison of the Daluxiang and Maoniuping carbonatitic REE deposits with Bayan Obo REE deposit, China. Lithos 106:12–24

Young BN, Parsons I, Threadgould R (1994) Carbonatite near the Loch Borralan Intrusion, Assynt. J Geol Soc Lond 150:945–954